REPORT NO. FRA-ORD&D-74-20
FRA-73-4

INPUT POWER CHARACTERISTICS OF A THREE-PHASE THYRISTOR CONVERTER

Raymand A. Wlodyka
Joseph D. Abbas
George Ploetz

OCTOBER 1973
FINAL REPORT

Prepared for
DEPARTMENT OF TRANSPORTATION
FEDERAL RAILROAD ADMINISTRATION
Office of Research, Development, and Demonstrations
Washington DC 20591

NOTICE

This document is disseminated under the sponsorship of the Department of Transportation in the interest of information exchange. The United States Government assumes no liability for its contents or use thereof.

TECHNICAL REPORT STANDARD TITLE PAGE

1. Report No.	2. Government Accession No.	3. Recipient's Catalog No.
FRA-ORD&D-74-20		

4. Title and Subtitle	5. Report Date
INPUT POWER CHARACTERISTICS OF A THREE-PHASE THYRISTOR CONVERTER	October 1973
	6. Performing Organization Code
7. Author(s) Raymand A. Wlodyka, Joseph D. Abbas, George Ploetz	8. Performing Organization Report No. DOT-TSC-FRA-73-4
9. Performing Organization Name and Address Department of Transportation Transportation Systems Center Kendall Square Cambridge MA 02142	10. Work Unit No. RR405/R4308
	11. Contract or Grant No.
	13. Type of Report and Period Covered Final Report Jan. 1972 - Dec. 1972
12. Sponsoring Agency Name and Address Department of Transportation Federal Railroad Administration Office of Research, Development, and Demons. Washington DC 20591	14. Sponsoring Agency Code

15. Supplementary Notes

16. Abstract

A phase delay rectifier operating into a passive resistive load was instrumented in the laboratory. Techniques for accurate measurement of power, displacement reactive power, harmonic components, and distortion reactive power are presented. The characteristics of the phase delay rectifier operating with unfiltered and inductively filtered resistive loads are presented using both derivations and measurements. The changes of the phase delay rectifier characteristics with a free wheeling diode in the circuit are also presented.

17. Key Words	18. Distribution Statement
· Rectifier, Phase Delay · Power Measurements, Three-Phase · Analysis, Harmonic	DOCUMENT IS AVAILABLE TO THE PUBLIC THROUGH THE NATIONAL TECHNICAL INFORMATION SERVICE, SPRINGFIELD, VIRGINIA 22151.

19. Security Classif. (of this report)	20. Security Classif. (of this page)	21. No. of Pages	22. Price
Unclassified	Unclassified	90	

Form DOT F 1700.7 (8-69)

PREFACE

The work described in this report was performed in the Power and Propulsion Branch at the Transportation Systems Center under the sponsorship of the Advanced Systems Division of the Office of Research, Development, and Demonstrations, Federal Railroad Administration. The objective of this work was to determine experimentally the power characteristics of the phase delay rectifier converter.

TABLE OF CONTENTS

LIST OF ILLUSTRATIONS

LIST OF ILLUSTRATIONS (CONT'D)

LIST OF ILLUSTRATIONS (CONT'D)

LIST OF TABLES

SYMBOLS AND ABBREVIATIONS

A	amperes
AC	alternating current
D	diode
DC	direct current
E_{ave}	average voltage
E_d	DC voltage
E_{do}	theoretical maximum DC voltage
E_p	peak voltage
E_x	voltage loss
EMF	electromotive force
e(t)	instantaneous voltage
FWD	free-wheeling diode
$F(\alpha)$	phase control factor
I	current
I_d	DC load current
I_{dc}	load current
I_L	line current
I_1	RMS value of 1st harmonic
I_ϕ	phase current
j	$\sqrt{-1}$
L	inductance
L_c	commutating inductance
n	order of the harmonic
P	power, real power
P_{ave}	average power

P_{eff}	effective power
PDR	phase delay rectifier
pf	power factor
Q	reactive power
Q_h	distortion reactive power
Q_p	displacement reactive power
Q_t	total reactive power
R	resistance
RMS	root mean square
S	apparent power
SCR	silicon controlled rectifier
T	period of the wave
t	time (seconds)
V	voltage
V_{dc}	DC voltage
V_ϕ	phase voltage
W_1	wattmeter 1
W_2	wattmeter 2
X	reactance
X_c	commutating reactance
X_l	line reactance
α	phase delay angle
μ	commutating angle
ϕ	phase angle
Ω	ohms
ω	angular frequency

1. INTRODUCTION

An important factor to consider in the design of any power system is its impact on the power distribution system. This report presents the results of a test program conducted at the Transportation Systems Center (TSC), in which the characteristics of a phase delay rectifier and its interface with the AC power source were investigated.

The phase delay rectifier (PDR) is used to convert fixed voltage and frequency AC power to a variable voltage DC. For traction applications, the AC voltage is usually a three-phase, three-wire system, and the usual rectifier system is the six-thyristor full-wave bridge. The DC output voltage for this bridge circuit can be adjusted from zero to full output by controlling the conduction intervals of the thyristors.

The objective of the study was to determine the effects of different load configurations on power, power factor and harmonic distortion. Load configurations included the unity power factor and reactive power factor cases, both with and without a free-wheeling diode. The particular load configurations were chosen because they represent the probable conditions present in the transit environment.

The inductor in most studies of rectifier circuits is assumed to be infinite so that there is consequently no ripple in the DC output. The PDR is also assumed to be bilateral; that is, the power can flow from either the AC source to the load, or vice versa, with the load becoming a source. For high power applications in high speed ground transportation, the physical size of the required inductor may rule out the ideal, and many load configurations also preclude the operation of the PDR in the bilateral mode. This investigation was directed toward analyzing the effect of the PDR when driving less than ideal loads. The theoretical case of infinite inductance is nevertheless summarized in this report.

Because of the non-sinsoidal nature of the currents and voltages in the PDR, these parameters have high harmonic content. When the load is purely resistive, the harmonic contents of the load voltage and current are the same. When inductance is added in series with the load, the impedance seen by the harmonics increases, and the output ripple is consequently reduced. Since the load is supplied from a three-wire source, and line currents are neither sinusoidal nor uni-directional, the harmonic content of the line current is high even though the load is ripple-free.

Because of the non-uniform waveforms and the phase displacement between the voltage and current, the suitability of the proposed instrumentation had to be verified. The resistance (or unity power factor) load case was examined in the laboratory. The output characteristics for the unity power factor case were also determined analytically and compared to the lab results to verify techniques and procedures. The close agreement between measured and calculated characteristics verified the suitability of the instrumentation and the procedure. The intermediate conditions of finite resistance and inductance were then set up in the lab and data collected and plotted. The effect of series impedance and of the addition of a free-wheeling diode for bypassing reactive current were also investigated, and their effects on the operation of the PDR noted. Results of these analyses and tests are presented in this report.

2. DESCRIPTION

The power electronics section of the PDR is shown schematically in Figure 2-1. The resistor, inductor and diode are shown as they were connected when included in any of the particular tests. There are two power thyristors connected between each of the three-phase input lines and the PDR output terminals. The gating of the thyristors is controlled so that the AC source voltage is rectified and current flow in the load is unidirectional. For the unfiltered resistive load, in which there is no additional energy storage, current will only flow if the anode voltage of a gated odd number thyristor is more positive than the cathode voltage of a gated even number thyristor. When the line to line voltage across a conducting thyristor pair falls to zero, the two thyristors will turn-off (or "commutate"). The load current falls to zero even though that pair may be receiving gate signals. Commutation brought about by the natural fall of the current or

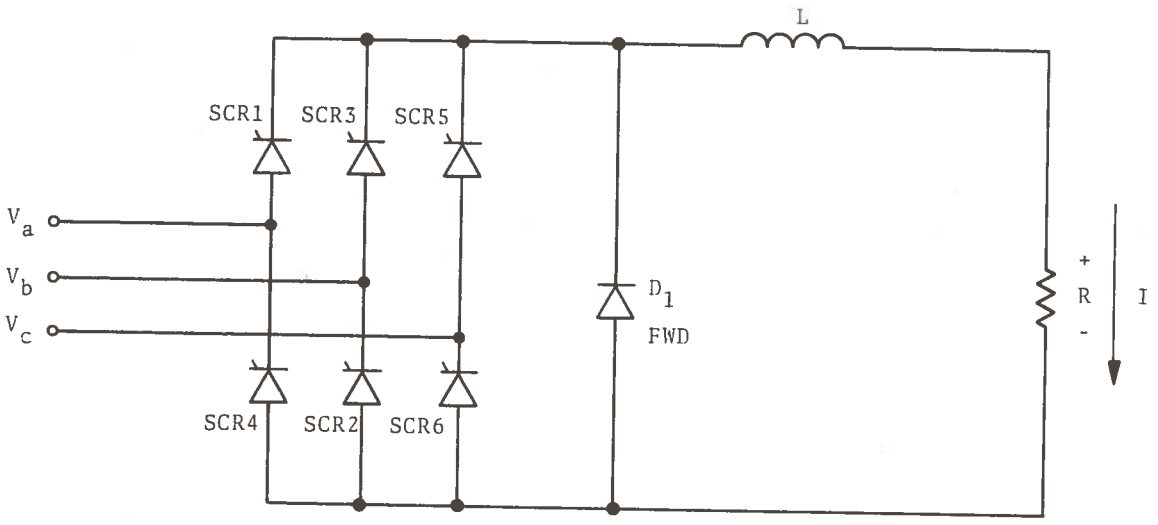

Figure 2-1. Power Electronics Schematic

voltage to the thyristor extinguishing point is called natural commutation. Forced commutation of the PDR thyristors occurs when a thyristor in another line is gated on and reverse-biases the original thyristor. In that case, the load current does not fall to zero but transfers from one thyristor to another. Both types of commutation occur in the PDR. The PDR will commutate naturally and its output voltage will fall to zero when gate signals are removed from all the tyristors. This characteristic allows for subcycle shutdown in the event of load or output system irregularities.

The addition of energy storage in the PDR circuitry changes its performance from that of the resistive load case. With inductance in either the load or source lines, the thyristors will continue to conduct until the energy stored in the inductor's magnetic field is dissipated. With capacitance in the load, the thyristors will commutate when the input voltage drops below the voltage stored on the capacitor.

The six power thyristors in Figure 2-1 are numbered in their conduction sequence for the line to line phase rotation shown. Phase A is designated the reference phase. Timing for the circuit is initiated every time the Phase A line to neutral voltage becomes the most positive of the three phase voltages.

Figure 2-2a shows the three-phase line to neutral voltages with V_{a-n}, the reference voltage, becoming most positive at time t=0. At that time in each cycle a precise delay period is initiated in the gate delay circuitry. At the conclusion of this delay period, thyristor 1 is triggered. The gate trigger logic then triggers the other five thyristors in sequence at 60° intervals. If the delay time is not changed before the start of the next "A" phase cycle, the trigger pulses for the thyristors occur at the same point in the cycle as before. If the delay time is changed, then the trigger pulses for all of the thyristors will be shifted in time by equal amounts. The delay interval of the PDR trigger pulse is the time expressed as the phase angle in degrees that each thyristor trigger is delayed. It is measured from the point of the input voltage waveform where that thyristor begins to hold off forward voltage.

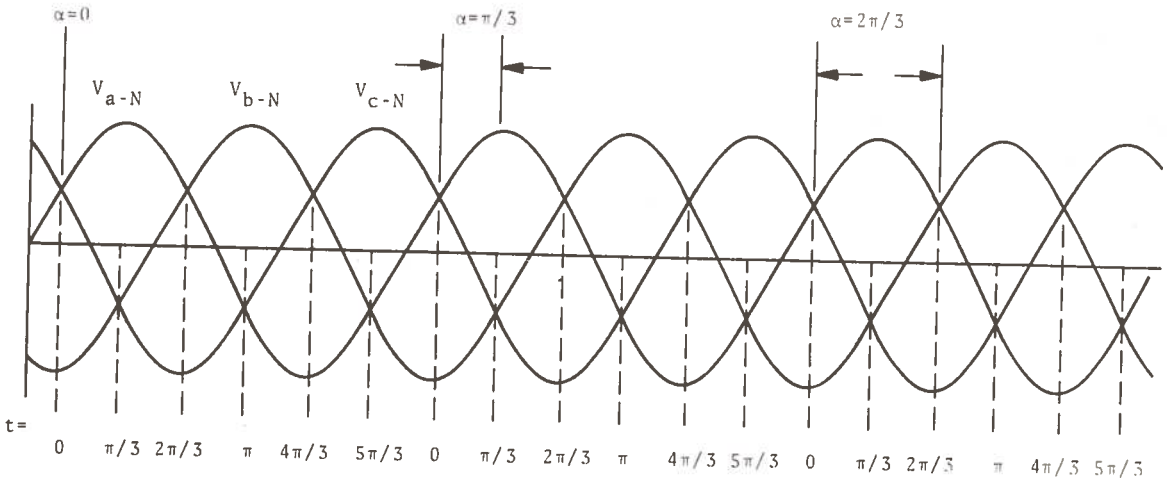

(a) Voltage Waveforms

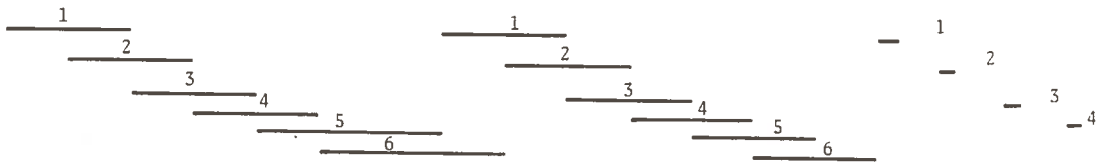

(b) Conducting Thyristors

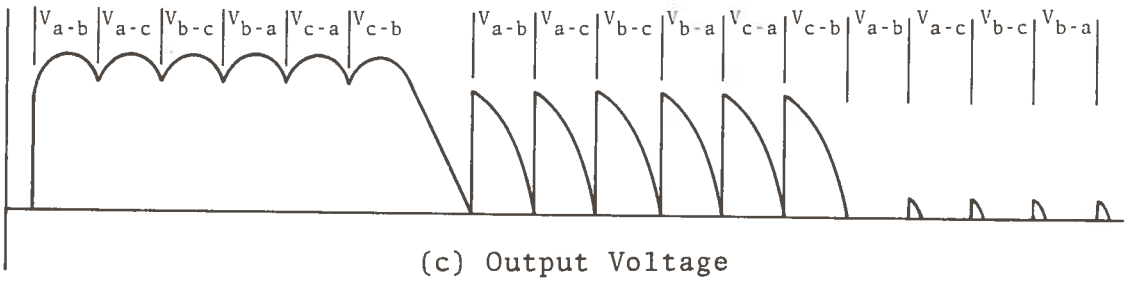

(c) Output Voltage

Figure 2-2. Voltage Waveforms

Figure 2-2b shows period of time each thyristor conducts for three cycles of operation, beginning with all off prior to t=0. The effects of changing the delay angle (α) in successive cycles is shown in Figure 2-2c, where the output voltage across a resistive load is constructed.

For the first cycle of operation, the delay angle (α) is 0° and the output voltage is at a maximum. At the start of the second cycle, the delay angle is suddenly increased to 60°, the gate trigger pulse to thyristor 1 is delayed and thristor 5 continues

to conduct. At 60° into the second cycle, the line voltage V_{c-b} across thyristors 5 and 6 is zero and they commutate. At that point, thyristors 1 and 6 are gated on and the line to line voltage V_{a-b} is impressed across the load. Since thyristor firings are all delayed to later points in the cycle where the line to line voltages are lower, the average output voltage is reduced and ripple is increased. The third cycle shows the effect of increasing the delay angle to angles approaching 120°. At these larger delay angles, the thyristors extinguish when the line to line voltage across them is zero. The conduction intervals, and hence the output voltage, approach zero.

3. TEST APPARATUS AND CHARACTERISTIC SOURCE IMPEDANCE

Prior to testing the PDR, the line source impedance was measured using the test setup shown schematically in Figure 3-1. With the switch S in position A, the source is open circuited, and the voltmeter, V, reads the source open circuit voltage, V_{OC}. With S1 in position B, the load is primarily inductive and the voltage due to the resistive component may be neglected. The series line reactance can now be determined from:

$$X_{L-L} = \frac{V_{OC}-V_L}{I} \qquad \text{(Equation 3-1)}$$

Similarly, the series line resistance can be determined with S1 in position C. The load in this case is resistive and the voltage due to the inductive component may be neglected.

$$R_{L-L} = \frac{V_{OC}-V_R}{I} \qquad \text{(Equation 3-2)}$$

Substituting the appropriate recorded values into these equations, we can solve for the source impedance:

$$X_{L-L} = \frac{V_{OC}-V}{I_L} \qquad R_{L-L} = \frac{V_{OC}-V}{I_R}$$

$$X_{L-L} = \frac{0.6V}{20A} = 0.03\Omega \qquad R_{L-L} = \frac{2.20V}{17.4A} = 0.126\Omega$$

$$X_a = X_b = 0.015\Omega \qquad R_a = R_b = 0.063\Omega$$

$$\therefore Z_{source} = R + jX = 0.063 + j\ 0.015$$

The reactive component of source impedance was also determined by using another method, that is, the measured value of commutation angle. When driving a load with a large inductive filter, the output current is almost ripple free. Without commutating reactance, the line current pulses would be rectangular because of the instantaneous current transfer from one line to another. But because of the reactances, this current transfer is not instantaneous.

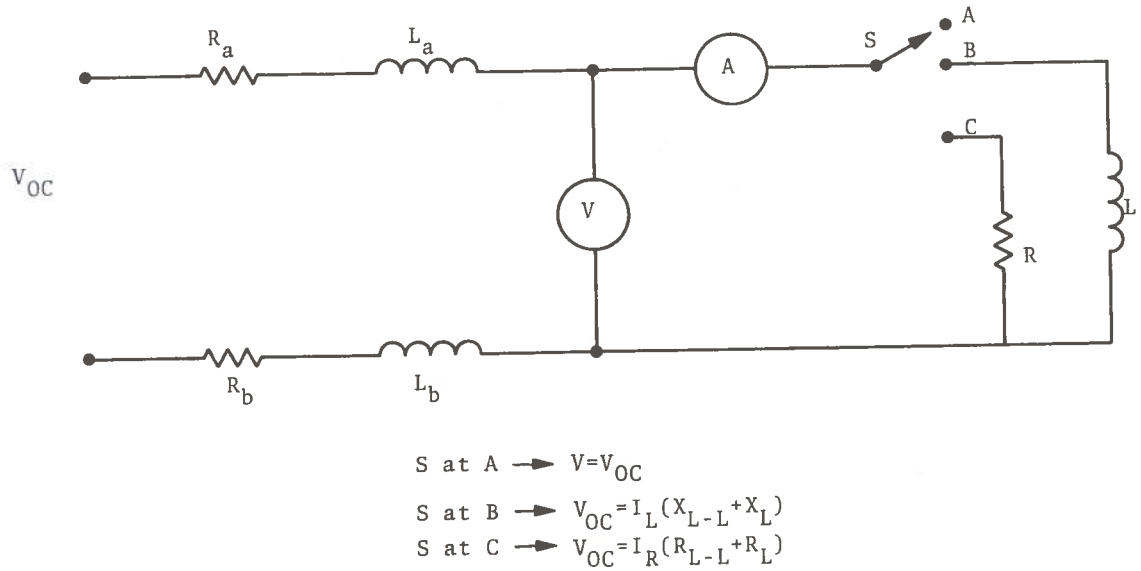

Figure 3-1. Schematic Showing Instrumentation for Measurement of Line Source Impedance

During the commutating interval, two thyristors are on simultaneously and the two lines are short circuited through the line reactances. The line reactance in each line can therefore be computed by making use of the measured voltage, current and commutation angle.

For the PDR in the laboratory, the source reactance was found by using the waveforms shown in Figure 3-2. This figure shows the line to line input voltage at two delay angles, $\alpha=10°$ and $\alpha=20°$. The commutation angle (μ) can be read from these waveforms. The measured values of voltage and current used to calculate the reactance are listed in Table 3-1.

The average output voltage is reduced because of the losses in the line reactance during switching. These losses can be computed from the inductive volt-ampere relationships and the measured values in Table 3-1. The volt-seconds absorbed by the commutating reactance can be found from:

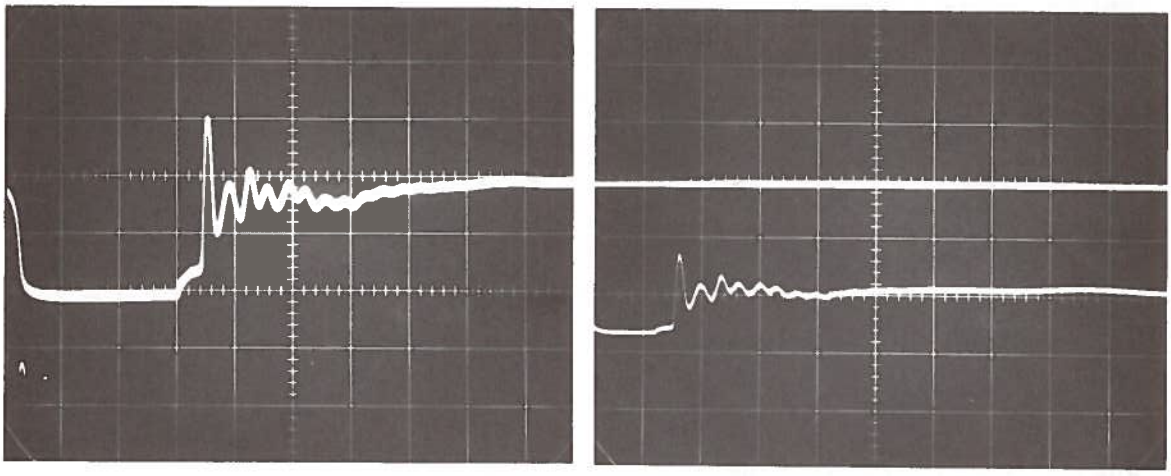

(a) α=10° (b) α=20°

Figure 3-2. Line to Line Voltage During Commutation Interval

$$L_c I_d = E_x \frac{T}{6} \qquad \text{(Equation 3-3)}$$

where: L_c = commutating inductance (line reactance)

I_d = DC load current

E_x = voltage loss

T/6 = time interval between commutations.

The voltage loss E_x can be calculated from measured values of the delay angle and commutation angle. Without commutation loss, the output voltage for low delay angles is

$$E_d(\alpha) = E_{do} \cos \alpha \qquad \text{(Equation 3-4)}$$

With commutation loss, the output voltage becomes

$$E_d(\alpha+\mu) = \frac{E_{do}\left(\cos \alpha + \cos (\alpha+\mu)\right)}{2} \qquad \text{(Equation 3-5)}$$

subtracting 5 from 4 we have an expression for E_x:

$$E_x = E_{do} \frac{(\cos \alpha - \cos (\alpha+\mu))}{2} \qquad \text{(Equation 3-6)}$$

from which

$$L_c = \frac{E_x}{I_d} \frac{T}{6}$$

For the conditions in Figure 3-2, the commutating inductance can be found by using the parameters in Table 3-1. The commutating angle is calculated from the following formula:

$$\mu = (t \text{ sec})(60 \text{ cycles/sec})(360 \text{ deg/cycle})$$

$$\mu = \left(21.6 \times 10^3\right) t \text{ degrees}$$

The magnitude of E_{do} used in these calculations, measured at light load and including diode drops, is 279V. The magnitude of the subsequently calculated commutating reactance is 0.019Ω. This figure compares favorably with the statically determined value of 0.015Ω obtained previously.

TABLE 3-1 COMMUTATING REACTANCE

$$\frac{T}{6} = \frac{16.66}{6} \times 10^{-3} = 2.77 \times 10^{-3}$$

Fig	I_d	α	μ	E_x	L_c	X_c
A	8.2	10°	.367°	.1535	52.2μh	0.197Ω
B	7.88	20°	.162°	.1395	49μh	0.185Ω

α	cos α	cosα(α+μ)	$\frac{\cos\alpha+\cos(\alpha+\mu)}{2}$	E_x	$\frac{E_x}{I_D}$	L_c
10°	.9848	.9837	5.5×10^{-4}	.1535	1.87×10^{-2}	52.2μh
20°	.9397	.9387	5×10^{-4}	.1395	1.77×10^{-2}	49μh

For the PDR experiments in the laboratory, the test equipment was connected as shown in Figure 3-3. The voltmeters and ammeters are Weston Series 900. The wattmeters are Hallmark Type 2 electrodynamometer single-phase meters. Harmonic analysis was performed with a manually tuned General Radio wave analyzer Model 1900A. A Hall effect transducer was used as a current probe in one of the AC lines. The buffered output of the probe served as the waveform source for the wave analyzer and the oscilloscope photographs. Its output also served as the input to an RMS converter, from which the RMS line current measurements were made.

Since the purpose of the test program was to characterize the PDR and not to stress the components, the thyristors and load components were selected so that they would be operated conservatively. Except for the measurement of series line reactance, the output current was kept below 10 A_{dc}. The resistance element used was a slide wire potentiometer set at 30Ω. This value of resistance was chosen primarily because the smoothing inductor available had a 60 HZ reactance of 30Ω. 30Ω was then chosen as the base impedance

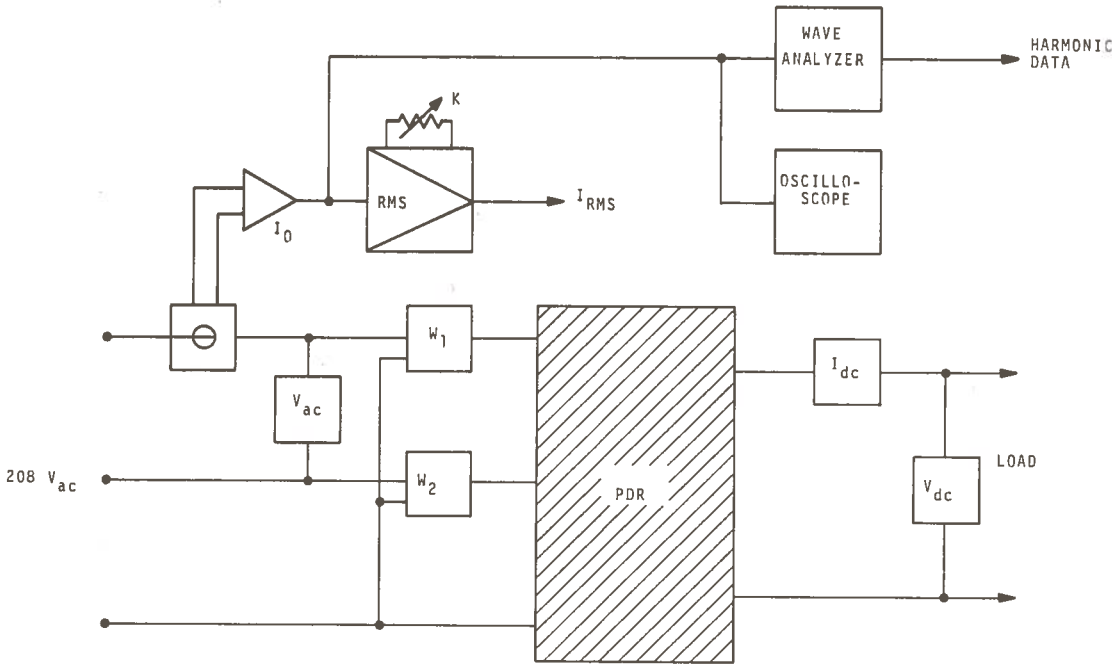

Figure 3-3. Schematic of Test Equipment Connection

from which all the per unit quantities used in the following sections of this report were calculated.

A more detailed discussion of the types of instrumentation to be used and the reasons for their selection is presented in the Appendix.

4. RESISTIVE LOAD OPERATION

For an unfiltered resistive load on the PDR, the output voltage and current waveforms are identical and in phase. Laboratory measurement of RMS voltage, RMS current, power and power factor are easily verified by analytical means. The comparison of these laboratory measurements with the analytical derivations provides a means of verifying the experimental techniques and equipment.

The measured and derived quantities are listed in Tables 4-1 and 4-2. Normalized values for each parameter are included in these tables, along with the measured values. The normalizing factor used for each parameter is the maximum calculated value, that is, the calculated value at $\alpha=0°$. In all cases, the measured and calculated values are close enough to verify the experimental technique. This will become evident in the curves that are presented in the following sub-sections. In these sub-sections, each of the critical parameters is discussed and a curve is presented showing the variation of each parameter as a function of delay angle. A short derivation of the equation used to calculate each parameter is also included.

4.1 OUTPUT VOLTAGE

The phase delay rectifier output voltage is a function of the delay angle. The measured output voltage for varying delay angles and the data is recorded in Table 4-1 column 2. This dependence of voltage on delay angle is shown pictorially in Figure 4-1.

From Figure 2-2c it is evident that the PDR output voltage consists of a series of pulses derived from the three-phase line to line voltages. The six power thyristors are triggered sequentially at one sixth cycle intervals, resulting in pulses which have identical waveshapes due to the symmetry of the line voltages. The average output voltage is controlled by varying the point in the cycle at which each of the thyristors is triggered. With a resistive load, the instantaneous output voltage is either zero,

TABLE 4-1 MEASURED AND NORMALIZED VALUES OF PARAMETERS FOR RESISTIVE LOAD

1 DELAY ANGLE (degrees)	2 VOLTAGE MEASURED	2 VOLTAGE NORMALIZED (÷271)	3 LINE CURRENT MEASURED	3 LINE CURRENT NORMALIZED (÷6.88)	4 POWER MEASURED	4 POWER NORMALIZED (÷2242)	5 APPARENT POWER MEASURED	5 APPARENT POWER NORMALIZED (÷2310)	6 REACTIVE POWER MEASURED	6 REACTIVE POWER NORMALIZED (÷1160)	7 POWER FACTOR
110	4	.014	.192	.027	10	.004	69.7	.016	74	.064	.143
100	15	.055	.66	.096	24	.011	230	.098	215	.185	.104
90	34	.132	1.31	.190	96	.043	457	.194	425	.366	.210
80	62	.228	2.08	.302	236	.102	725	.308	667	.574	.325
70	96	.353	2.88	.419	458	.203	1000	.425	930	.801	.458
60	135	.497	3.71	.540	738	.328	1300	.553	1070	.925	.560
50	176	.646	4.52	.656	1070	.476	1580	.672	1140	.985	.678
40	209	.770	5.24	.760	1424	.631	1820	.775	1190	1.03	.782
30	234	.862	5.72	.831	1704	.755	1990	.846	945	.814	.856
20	252	.927	6.14	.891	1950	.868	2140	.910	774	.666	.910
10	264	.972	6.33	.920	2114	.940	2210	.941	675	.580	.955
0	267	.982	6.40	.930	2164	.965	2230	.950	592	.510	.970

TABLE 4-2 CALCULATED AND NORMALIZED VALUES OF PARAMETERS FOR RESISTIVE LOAD

$Q_{MAX} = 1350$

α (deg.)	$f(\alpha)$	$\sqrt{f(\alpha)}$	E_d	I_L	P	ST	Q	p.f.	$\frac{E_d}{E_{MAX}}$	$\frac{I_L}{I_{MAX}}$	$\frac{P}{P_{MAX}}$	$\frac{ST}{ST_{MAX}}$	$\frac{Q}{Q_{MAX}}$
110	.002	.042	4.4	.308	5.2	111	111	.047	.016	.042	.002	.043	.082
100	.013	.114	17.0	.84	33.6	301	299	.112	.06	.117	.014	.116	.221
90	.045	.212	57.7	1.55	116	560	547	.207	.134	.216	.047	.217	.405
80	.103	.320	66	2.35	266	845	802	.315	.235	.328	.108	.327	.594
70	.190	.436	100	3.20	491	1152	1042	.426	.355	.446	.199	.446	.772
60	.307	.554	141	4.06	793	1464	1230	.542	.502	.566	.321	.566	.911
50	.449	.670	181	4.91	1160	1770	1337	.655	.644	.685	.469	.685	.990
40	.599	.774	218	5.68	1546	2045	1339	.756	.776	.792	.626	.791	.991
30	.740	.860	243	6.31	1911	2270	1225	.842	.865	.880	.773	.878	.907
20	.855	.925	264	6.78	2208	2445	1050	.903	.940	.946	.894	.946	.778
10	.930	.965	276	7.08	2401	2550	858	.942	.982	.987	.972	.987	.636
0	.957	.978	281	7.17	2471	2584	758	.956	1.00	1.00	1.00	1.00	.561

with no thyristors conducting, or the instantaneous line to line voltage impressed across it through a conducting thyristor pair.

The instantaneous voltage can be expressed as either:

$$e(t) = 0 \qquad \text{(Equation 4-1)}$$

or

$$e(t) = E_p \sin(\omega t + \phi) \qquad \text{(Equation 4-2)}$$

where:

$e(t)$ = instantaneous output voltage

E_p = peak value of the line to line voltage

ωt = electrical phase angle in radians

ϕ = phase angle of the gated line to line voltage.

The average value of output voltage can be found by integrating the instantaneous value over one complete cycle of operation. Thus,

$$E_{ave} = \left(\frac{1}{T}\right)\int_{o}^{T} e(t)\, dt \qquad \text{(Equation 4-3)}$$

where T = the period of one cycle in seconds.

For the steady state case, the six pulses are identical because of the symmetry of the waveform. The average value of the output now becomes:

$$E_{ave} = 6\left[\frac{1}{T}\int_{t=t_o}^{t=\frac{T}{6}} e(t)\, dt\right] \qquad \text{(Equation 4-4)}$$

Time for each cycle of operation is measured from the point where the reference-phase line to neutral sine wave becomes positive, but the phase delay angle (α) is measured from the time when that voltage becomes the most positive of the three voltages. That

point is 60° into the cycle. When the integration limits are changed to include that angle and the phase delay angle (α), Equation 4-4 becomes

$$E_{ave} = \frac{6}{T} \int_{\alpha+\frac{\pi}{3}}^{\theta_m} E_p \sin \omega t \, d(\omega t) \qquad \text{(Equation 4-5)}$$

where $T = \frac{2\pi}{\omega}$ = time for one cycle

$\theta_m = \alpha + \frac{2\pi}{3}$ for $0 < \alpha < \frac{\pi}{3}$

$\theta_m = \pi$ for $\frac{\pi}{3} < \alpha < \frac{2\pi}{3}$

This leads to two expressions for the output voltage because of the change in limits at $\omega t = \pi$, where the polarity reversal of the input voltage turns off the thyristors. At delay angles less than 60°, the conduction period during each pulse is 60°, but at delay angles greater than 60°, the conduction period is $\left(\frac{2\pi}{3}-\alpha\right)$ becoming zero at $\alpha = 120°$.

The solution of Equation 4-5 for delay angles less than 60° is

$$E_d = E_{ave} = \frac{3}{\pi} E_p \cos \alpha \qquad \text{(Equation 4-6)}$$

the theoretical maximum output voltage (E_{do}) at $\alpha=0$ is $E_{do} = \frac{3}{\pi} E_p$. For angles greater than 60°,

$$E_d = E_{ave} = \frac{3}{\pi} E_p \left[1 + \cos \left(\alpha+\frac{\pi}{3}\right)\right] \qquad \text{(Equation 4-7)}$$

At the crossover point, $\alpha = 60°$, both expressions are valid, they both yield the same value, hence there is no discontinuity in the plot of E_d vs α. In Figure 4-1, both the measured and the calculated values of E_d are plotted. It is evident that they agree favorably.

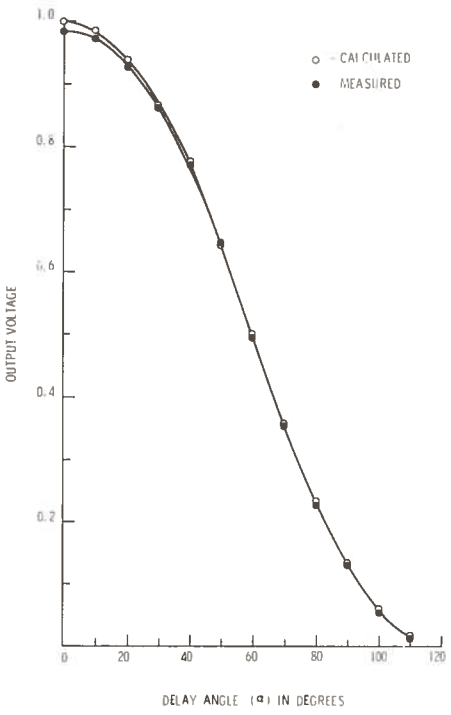

Figure 4-1. Output Voltage vs Delay Angle

4.2 LINE CURRENT

The line current drawn by the PDR is also dependent upon the phase delay angle. This is evident in Table 4-1, column 3, and also in Figure 4-2, where line current is plotted vs. delay angle. Waveforms of line currents for four different delay angles are shown in Figure 4-3. There are four current pulses per cycle; two positive pulses through the load, one to each of the other two lines, and two negative pulses through the load, one from each of the other lines. These pulses are segments of sinusoids developed from the sinusoidal line to line excitation. The effective value of these current pulses is:

$$I_{RMS} = \sqrt{\frac{1}{T}\int_{0}^{T} i(t)^2 \, dt} \qquad \text{(Equation 4-8)}$$

the instantaneous value of current for this case (pure resistance load) is given by:

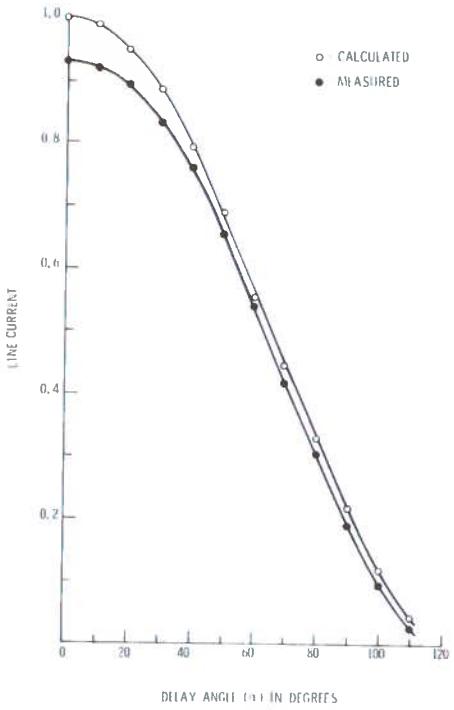

Figure 4-2. Line Current vs Delay Angle

$$i(t) = \frac{e(t)}{R}$$

e(t) consists of the six identical pulses derived from the three-phase line to line voltages. To determine the RMS line current, the expression that is to be evaluated must be written to include only the current pulses that flow in one line. These can be found by solving for i(t) using the expression previously derived for the voltage.

$$e(t) = E_p \sin \omega t \qquad \text{(Equation 4-9)}$$

where $\alpha + \frac{\pi}{3} < \omega t < \theta_m$

and $\theta_m = \alpha + \frac{2\pi}{3}$ for $0 < \alpha \leq \frac{\pi}{3}$

$\theta_m = \pi$ for $\frac{\pi}{3} \leq \alpha < \frac{2\pi}{3}$

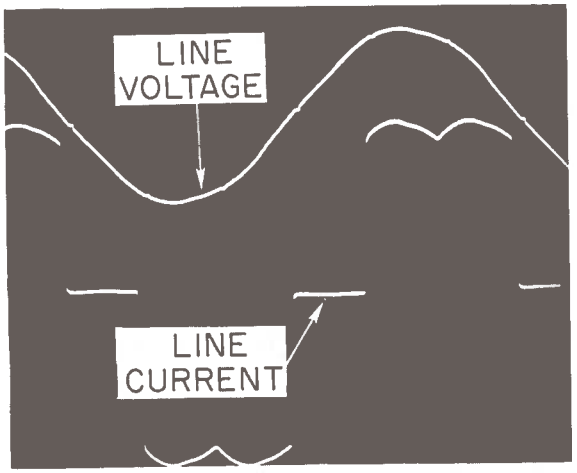

(a) α=10°

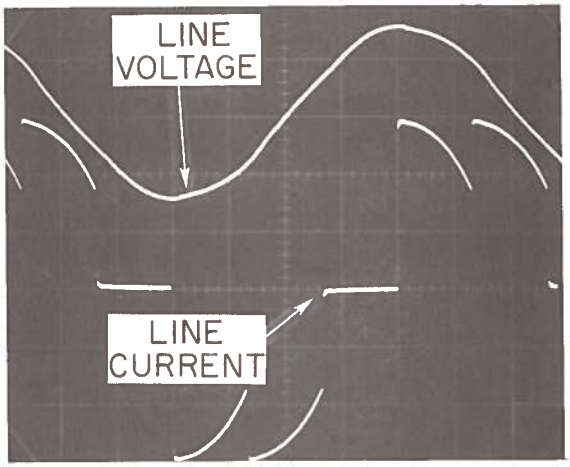

(b) α=30°

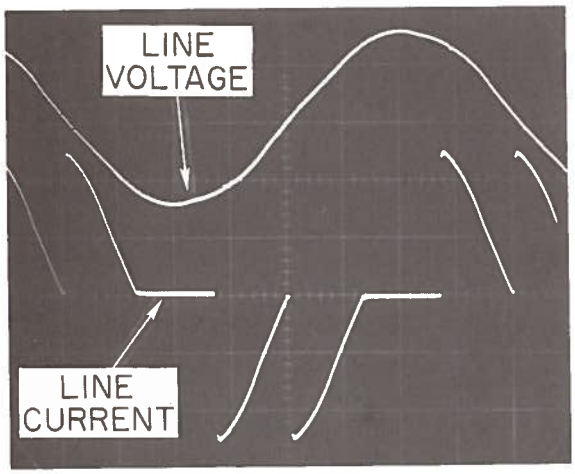

(c) α=60°

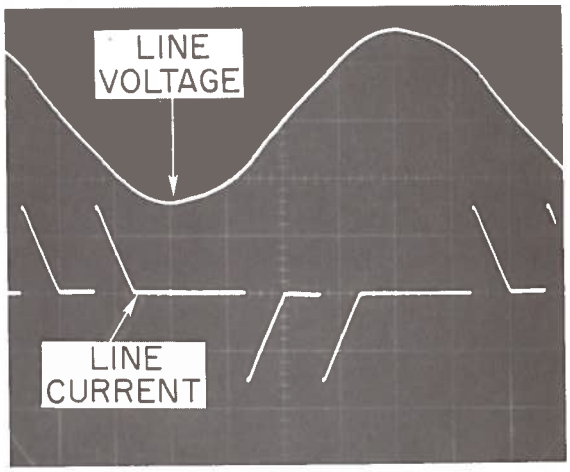

(d) α=90°

Figure 4-3. Line Waveforms Resistive Load

From Equation 4-8 we have

$$i(t) = \frac{E_p \sin \omega t}{R} \Bigg]_{\omega t=\alpha+\frac{\pi}{3}}^{\theta_m} \qquad \text{(Equation 4-10)}$$

For one cycle of line current there are four of these intervals, therefore the expression for the RMS value of the line current becomes:

$$I_L = I_{RMS} = \sqrt{\frac{4}{T} \int_{\alpha+\frac{\pi}{3}}^{\theta_m} \left(\frac{E_p}{R}\right)^2 \sin^2 \omega t \, dt} \qquad \text{(Equation 4-11)}$$

Performing the integration for $T = \frac{2\pi}{\omega}$ yields:

$$I_L = I_{RMS} = \frac{E_p}{R} \sqrt{\frac{2}{\pi} \left[\frac{\omega t}{2} - \frac{1}{4} \sin 2\omega t\right]}_{\alpha+\frac{\pi}{3}}^{\theta_m} \qquad \text{(Equation 4-12)}$$

The line current value as a function of the delay angle α, calculated from Equation 4-12, using the circuit constants are also included in Figure 4-2.

4.3 PHASE CONTROL FACTOR

The derivation of the RMS line current includes the solution to a definite integral. This solution is used in further derivations of the PDR characteristics with a pure resistive load and is designated the phase control factor, $f(\alpha)$:

$$f(\alpha) = \left[\frac{\omega t}{2} - \frac{1}{4}\sin 2\omega t\right]_{\omega t=\alpha+\frac{\pi}{3}}^{\omega t=\theta_m}$$

$$\theta_m = \alpha + \frac{2\pi}{3} \text{ for } 0 < \alpha < \frac{\pi}{3}$$

$$\theta_m = \pi \text{ for } \frac{\pi}{3} < \alpha < \frac{2\pi}{3} \qquad \text{(Equation 4-13)}$$

The solution yields two terms for $f(\alpha)$:

$$\text{for } 0 < \alpha < \frac{\pi}{3} \quad f(\alpha) = \frac{\pi}{6} + \frac{\sqrt{3}}{4}\cos 2\alpha \qquad \text{(Equation 4-14)}$$

$$\text{for } \frac{\pi}{3} < \alpha < \frac{2\pi}{3} \quad f(\alpha) = \frac{\pi}{3} - \frac{\alpha}{2} + \frac{\sqrt{3}}{4}\cos 2\alpha - \frac{1}{8}\sin 2\alpha$$

$$f(\alpha) = \frac{\pi}{3} - \frac{\alpha}{2} + \frac{1}{4}\cos\left(2\alpha + \frac{\pi}{6}\right)$$

(Equation 4-15)

Table 4-2 includes a tabulation of $f(\alpha)$ and $\sqrt{f(\alpha)}$ in columns 2 and 3, for ten degree increments of α. Figure 4-4 is a plot of these functions vs α.

The RMS line current derived in the previous section can be re-written as

$$I_{RMS} = \frac{E_p}{R}\sqrt{\frac{2}{\pi} f(\alpha)} \qquad \text{(Equation 4-16)}$$

4.4 POWER

The measured variation of power with changes in delay angle for the PDR is tabulated in Table 4-1, column 4, and shown graphically in Figure 4-5.

The power delivered to the load can be calculated by integrating the instantaneous power for one cycle of operation.

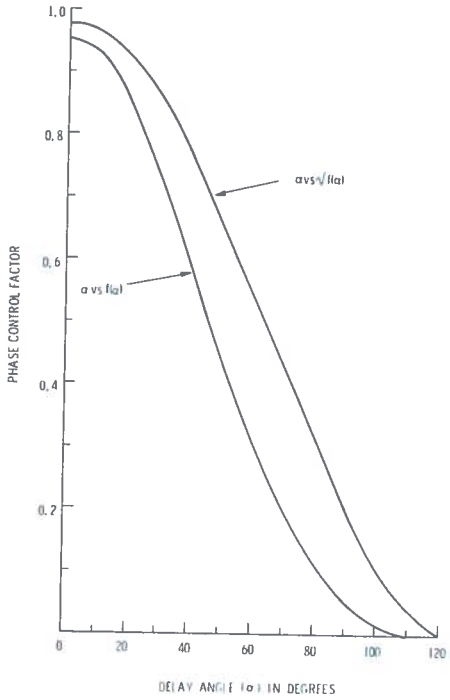

Figure 4-4. Phase Control Factor vs Delay Angle

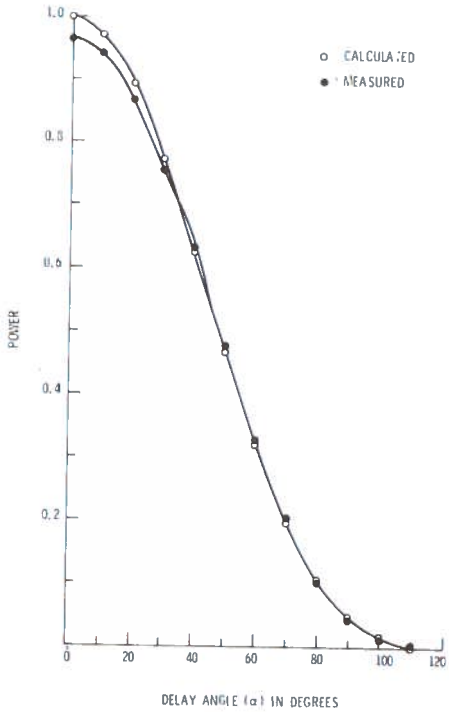

Figure 4-5. Power vs Delay Angle

$$P_{av} = \frac{1}{T}\int_{o}^{T} e(t) \cdot i(t)\, dt \qquad \text{(Equation 4-17)}$$

Figure 2-2c shows how segments of sinusoids combine to produce the direct output with six symmetrical intervals per cycle. Photographs of the six-pulse output voltage waveform taken at four different delay angles are shown in Figure 4-6. Since each cycle contains six equal intervals, the equation for average power can then be written as:

$$P = \frac{6}{T}\int_{t=t_o}^{\frac{T}{6}} e(t) \cdot i(t)\, dt \qquad \text{(Equation 4-18)}$$

Without filtering:

$$i(t) = \frac{e(t)}{R} \qquad \text{(Equation 4-18a)}$$

Substituting for i(t) Equation 4-18 becomes

$$P = \frac{6}{T}\int_{t=t_o}^{t=\frac{T}{6}} \frac{[e(t)]^2}{R}\, dt \qquad \text{(Equation 4-19)}$$

Insertion of integration limits which include the effects of delay angle (α) and the expression for e(t), Equation 4-19 becomes

$$P = \frac{6}{T}\int_{\alpha+\frac{\pi}{3}}^{\theta_m} \frac{\left(E_p\right)^2}{R} \sin^2 \omega t\, d\omega t$$

$$T = \frac{2\pi}{\omega}$$

$$\theta_m = \alpha + \frac{2\pi}{3} \quad \text{for } 0 < \alpha < \frac{\pi}{3}$$

$$= \pi \qquad \text{for } \frac{\pi}{3} < \alpha < \frac{2\pi}{3} \qquad \text{(Equation 4-20)}$$

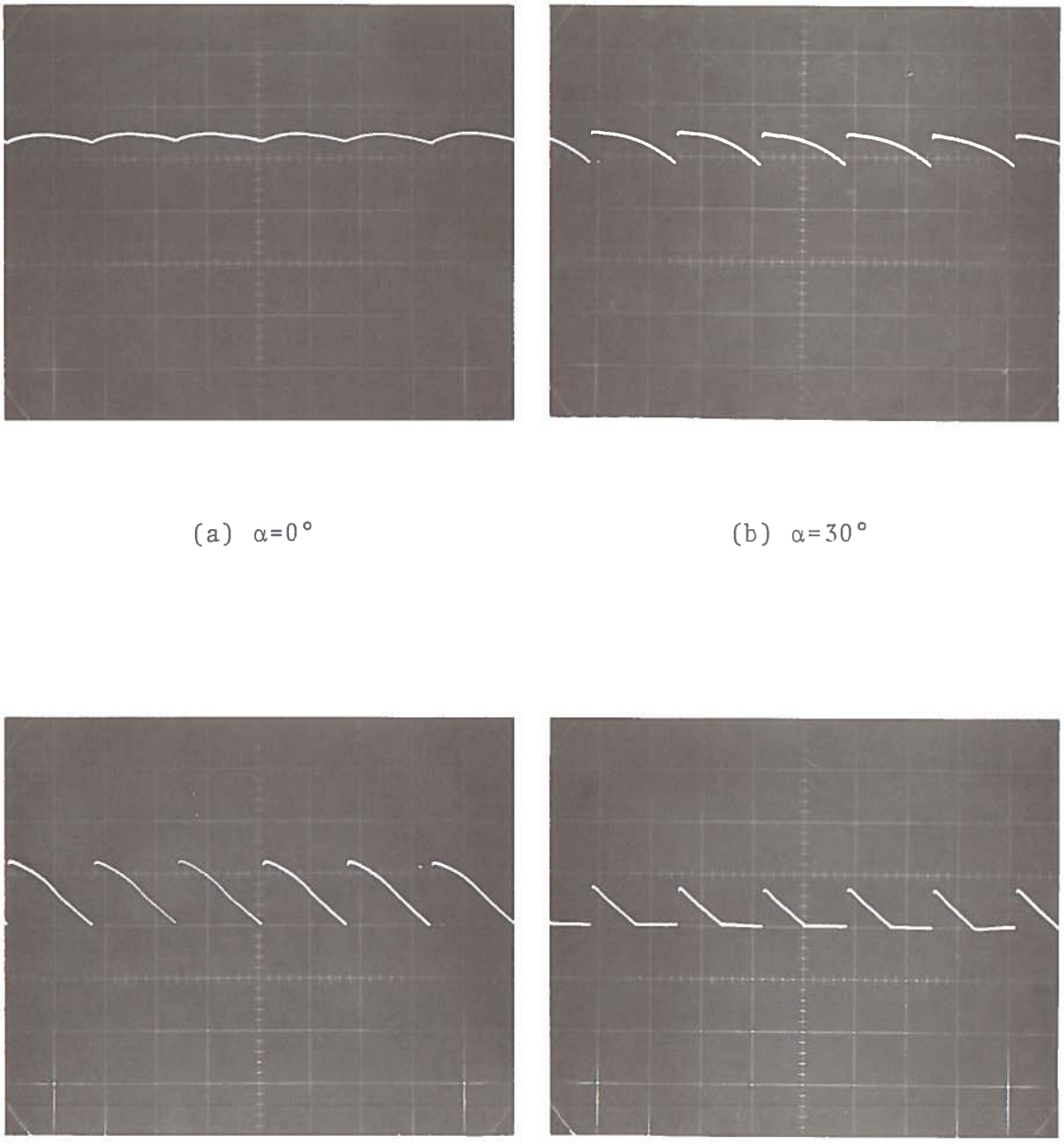

(a) $\alpha=0°$ (b) $\alpha=30°$

(c) $\alpha=60°$ (d) $\alpha=90°$

Figure 4-6. Output Voltage into Resistive Load

After performing the integration

$$P = \frac{\left(E_p\right)^2}{R}\left[\frac{3}{\pi}\right]\left[\frac{\omega t}{2} - \frac{1}{4}\sin 2\,\omega t\right]_{\alpha+\frac{\pi}{3}}^{\theta_m} \qquad \text{(Equation 4-21)}$$

The power can now be expressed in terms of the phase control factor $f(\alpha)$

$$P = \frac{3\left(E_p\right)^2}{\pi R} f(\alpha) \qquad \text{(Equation 4-22)}$$

The calculated power and the measured power, normalized to the maximum calculated value of power, as a function of α, is presented in Figure 4-5.

4.5 APPARENT POWER

The measured values of apparent power as a function of delay angle are presented in Table 4-1, column 5, and shown graphically in Figure 4-7.

The formula for real power delivered to a load derived in the preceding section showed that the power into a fixed load is a function of the delay angle. Because load voltage and current are not sinusoidal, their instantaneous values must be integrated for one cycle to determine real power. The apparent power input however, is the sum of the products of RMS voltage and RMS current in each phase. For the three-phase system, the apparent power is

$$S = 3\,V_\phi I_\phi \,. \qquad \text{(Equation 4-23)}$$

If the line impedances are negligible, then the voltages at the inputs are the three-phase sinusoidal line to line and the RMS phase voltages are:

$$V_\phi = \frac{V_L}{\sqrt{3}} \qquad \text{(Equation 4-24)}$$

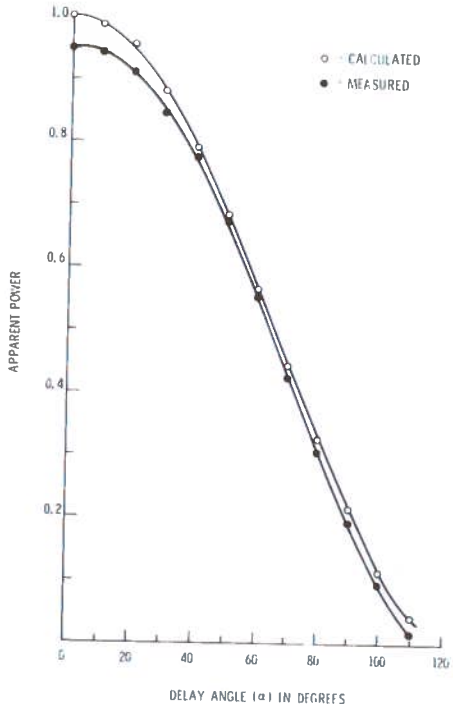

Figure 4-7. Apparent Power vs Delay Angle

The RMS phase current is the RMS line current, therefore the apparent power can be expressed as a function of the line to line voltage and current:

$$S = \sqrt{3}\, V_L\, I_L \qquad \text{(Equation 4-25)}$$

for sinusoidal voltage input,

$$V_L = \frac{E_p}{\sqrt{2}} \qquad \text{(Equation 4-26)}$$

$$I_L = I_{RMS} = \frac{E_p}{R} \sqrt{\frac{2}{\pi}\, f(\alpha)} \qquad \text{(Equation 4-27)}$$

Substituting Equations (4-26) and (4-27) into (4-25), the apparent power can be expressed as a function of the phase control factor:

$$S = \frac{E_p^2}{R}\sqrt{\frac{3}{\pi}\, f(\alpha)} \qquad \text{(Equation 4-28)}$$

hence

$$S = K\sqrt{f(\alpha)} \qquad \text{(Equation 4-29)}$$

where

$$K = \frac{E_p^2}{R}\sqrt{\frac{3}{\pi}}$$

Figure 4-7 also shows the variation of the calculated values of apparent power with delay angle, where it is evident that both the calculated values and measured values are very close.

4.6 REACTIVE POWER

The reactive power of a system is that power which contributes to the total volt-amperes, but does not contribute to the real (effective) power. For the PDR system, there are two phenomena which contribute to reactive power: the phase displacement between the fundamental components of voltage and current, and the harmonic distortion of the current waveform caused by the chopping action of the rectifier.

Since there are two sources of the total reactive power, they each must be measured separately. The reactive power due to the phase displacement of the fundamental voltage current waveforms was determined. This can be measured by two methods: by using watt-meter measurements, and by using volt-ampere measurements. By using the two-wattmeter method for power measurement, displacement reactive power is given by:

$$Q_p = \sqrt{3}\,(W_1 - W_2)$$

where W_1 and W_2 are the respective wattmeter readings.

The other component of reactive power is due to the distortion of the current waveform by the harmonics. The harmonic current magnitude was determined by the vectorial subtraction of the measured RMS line current and the measured RMS fundamental current.

$$I_d = \sqrt{I_L^2 - I_1^2}$$

from which

$$Q_h = \sqrt{3}\, V_L\, I_d$$

The total reactive power is now equal to the phasor sum of these two components.

$$Q_T = \sqrt{Q_p^2 + Q_h^2}$$

A pictorial representation of these phasor quantities, and how they fit into the system power phasor diagram is shown in Figure 4-8. These measured values of Q_T are listed in Table 4-1, column 6, and are shown graphically in Figure 4-9. The reactive power can also be calculated from the relationship:

$$Q_T = S \sin \theta$$

where

$$\theta = \cos^{-1} \frac{P}{S}$$

The curve for these calculated values is also shown in Figure 4-9 for comparison.

4.7 POWER FACTOR

Power factor is the ratio of total power input to total volt-amperes input to the PDR. That is, for the PDR, power factor is determined at the unit's AC line terminals. The measured values of both real and apparent power are included in Table 4-1. The power factor determined by taking the ratio of these two quantities is also included in Table 4-1, column 7, and shown graphically in Figure 4-10.

There is a power factor associated with the PDR even though there are no reactive components in the load. This power factor

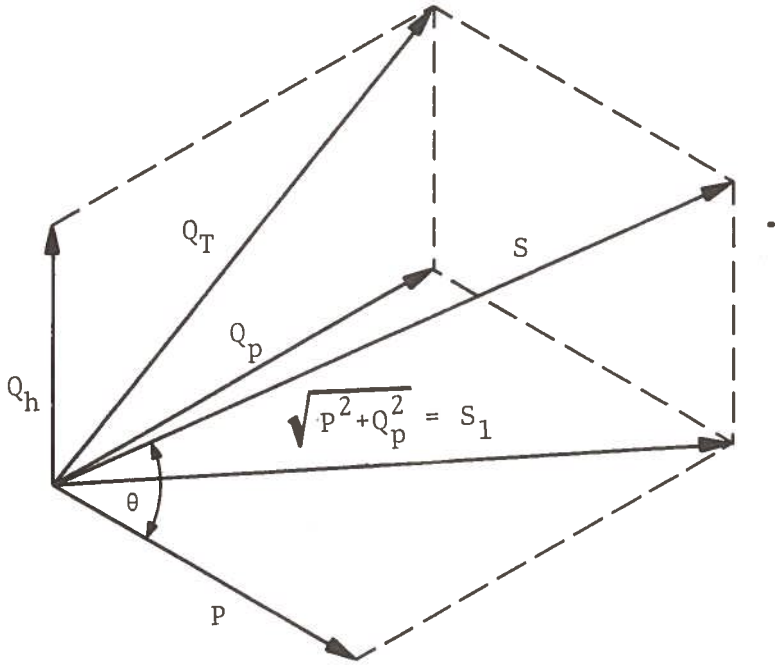

Figure 4-8. Phasor Resolution of the Power Components

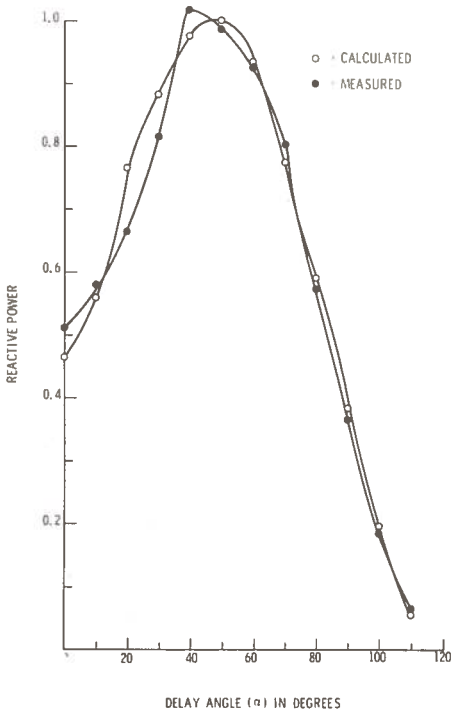

Figure 4-9. Reactive Power vs Delay Angle

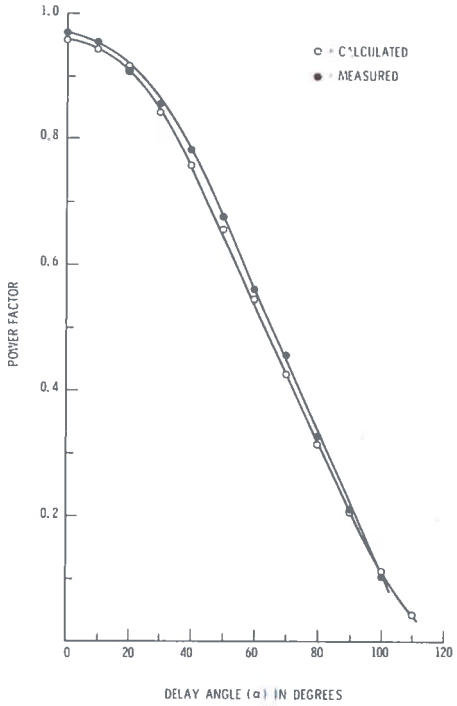

Figure 4-10. Power Factor vs Delay Angle

results from two phenomena:

a. The delay of thyristor turn-on causes the current and voltage to be out of phase, thereby resulting in a displacement component of power factor.

b. The chopping action of the PDR on the current waveform generates harmonic currents. These harmonics distort the current waveform and produce a distortion component of power factor.

Power factor has been determined by taking the ratio of the measured values of real and apparent power. Power factor can also be determined by taking the ratio of the previously calculated values of real and apparent power. Using Equation 4-22 for the real power and Equation 4-28 for the apparent power, we can derive power factor as:

$$pf = \frac{P}{S} = \frac{\frac{3E_p^2}{\pi R} f(\alpha)}{\frac{E_p^2}{R}\sqrt{\frac{3}{\pi} f(\alpha)}} = \sqrt{\frac{3}{\pi} f(\alpha)} \qquad \text{(Equation 4-30)}$$

The measured and calculated power factors are plotted in Figure 4-10, where it can be seen that the two curves are in close agreement.

4.8 HARMONICS

The chopping action of the PDR generates distortion currents which feed back onto the AC lines, resulting in line currents consisting of the 60 Hz fundamental and its harmonics. The magnitudes of the fundamental and its harmonics vary with phase control, and do not follow the simple $\frac{I}{n}$ relationship. The ratio of the harmonic currents to the fundamental current generally increases as the phase delay angle increases. The fundamental component as well as the harmonic components of the line current have been measured in the laboratory using a wave analyzer. The magnitudes of each have been recorded for delay angles from 0 to 120 degrees, and the results are shown in Figure 4-11. By plotting the harmonic magnitudes as percentages of the fundamental at each delay angle, the increased distortion with delay angle is better illustrated. The harmonic distortion is most severe at higher delay angles where the current pulses become discontinuous.

Not all harmonics are present in the six-pulse, three-phase system. The third harmonic and its multiples do not appear and also all even harmonics are not present. The lowest harmonic present is the fifth followed by the seventh, eleventh, thirteenth, etc. These harmonics can cause losses in the series line impedance of the input lines and excess currents in bypass capacitors, resulting in heating losses and counter-torques in generating equipment and interference in telecommunication and other audio equipment. Their effect on the characteristics of the PDR is manifested as a reduction of the system power factor. To minimize these harmonic effects, a typical PDR load will include output filtering. This condition will be described in a later section.

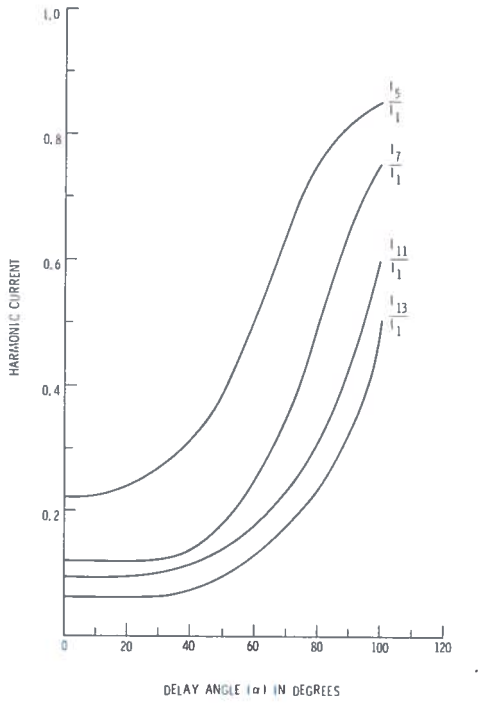

Figure 4-11. Harmonic Current vs Delay Angle

The harmonic currents are distortion currents which do not contribute to any real power. This can be shown by integrating the instantaneous power over a full cycle:

$$P = \frac{1}{T}\int_{o}^{T} e(t) \cdot i(t)\, dt \qquad \text{(Equation 4-31)}$$

For the cases where e(t) and i(t) are complex waveforms made up of fundamental and harmonic sinusoidal components, this expression can be expanded to

$$P = \frac{1}{T}\int_{o}^{T} \sum_{\substack{n=1 \\ m=1}}^{n,m} E_m \sin m(\omega t) \cdot I_n \sin\left[n(\omega t) + \theta_n\right] d(\omega t)$$

(Equation 4-32)

Where: E_m = harmonic voltage peak value

I_n = harmonic current peak value

θ_n = displacement angle.

This integral has a non-zero solution only for the cases where m and n are equal. If the line voltage is supplied from a stiff, low impedance bus such that it is free of harmonics, then m will only equal 1. The integral then has a solution for n=1; all other values of n result in a zero average output. This solution indicates that the only frequency that contributes to real power is the fundamental line frequency and not the harmonics.

The harmonics do contribute to the RMS line current vectorially:

$$I_L = \sqrt{\sum_{n=1}^{n} I_n^2} \qquad \text{(Equation 4-33)}$$

and since this RMS line current is used in the determination of apparent power and power factor, the presence of the harmonics results in a lower power factor for the system.

4.9 SERIES LINE REACTANCE

In the operation of the PDR in a transit environment, the distance between power sub-stations will have an impact on system performance. Losses in the source lines before the PDR reduce efficiency and decrease the maximum output voltage capability. The principal causes of line loss are line resistance and inductance. The resistance causes a system power loss and a line voltage drop which reduces voltage at the rectifier input terminals. The power loss lowers overall efficiency, while the voltage drop lowers the output voltage capability. The operational characteristics of the PDR are not altered by the line resistance, but it is desirable to minimize it from the standpoint of efficiency.

Inductive reactance in the source lines also lowers the output voltage, but unlike series resistance it alters the characteristics

of the converter itself. During a thyristor conduction period, energy is stored in the magnetic field of the line inductance. When another thyristor is switched on (to transfer the current to another line), this magnetic field collapses and induces a voltage in the line. Commutation of the off-going thyristor is delayed until all the energy stored in the line reactance has been dissipated. The inductive impedance in the second line also limits current build-up in the on-coming thyristor. The net result of the line reactances is that two thyristors are on simultaneously. The period of dual conduction is called the overlap angle (μ). Assuming balanced conditions, with two thyristors on and conducting through identical impedances, the output voltage becomes the average voltage between the two lines instead of the greater of the two. The series reactance thus causes a reduction of output voltage at any given delay angle.

Figure 4-12 shows the current and voltage waveforms as series reactance is increased at one delay angle (α=60°). The energy storage of the series reactance filters the line current in the same manner that inductance in the load does. The output current and output voltage waveforms are similar to those obtained with an inductive load. However, the dual thyristor conduction intervals lower the output voltage capability. The configuration of inductive filtering in the load is dealt with in a later section.

The smoothing of the current waveform is due to the attenuation of the higher harmonics by the input reactance. Without any inductance (Figure 4-12a) the line to line voltage, output voltage and output current are unchanged. As the series reactance increases, the line to line voltage at the input of the PDR distorts due to the increased overlap angle (μ). The per unit reactances used in this measurement include the series reactance in each of the three lines. The base impedance for calculating per unit quantities is the base impedance used to calculate the per unit load impedances for the PDR.

Table 4-3 lists the normalized output voltage as a function of α for the four load configurations pictured in Figure 4-12.

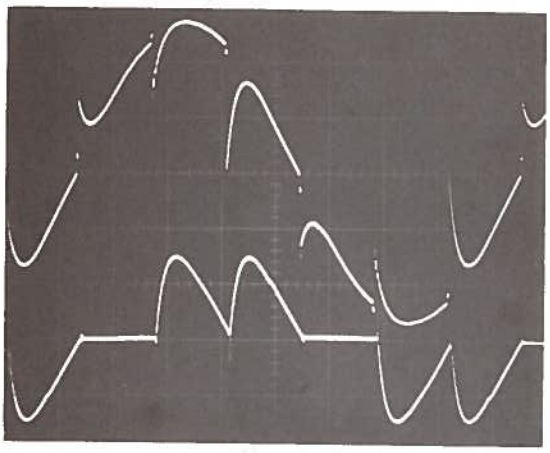

(a) 2Ω

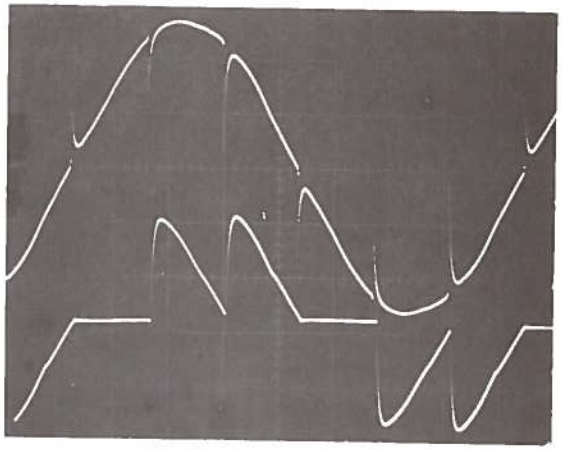

(b) 1Ω

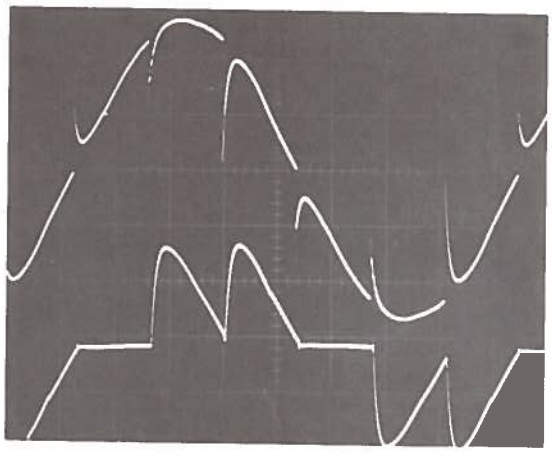

(c) .5Ω

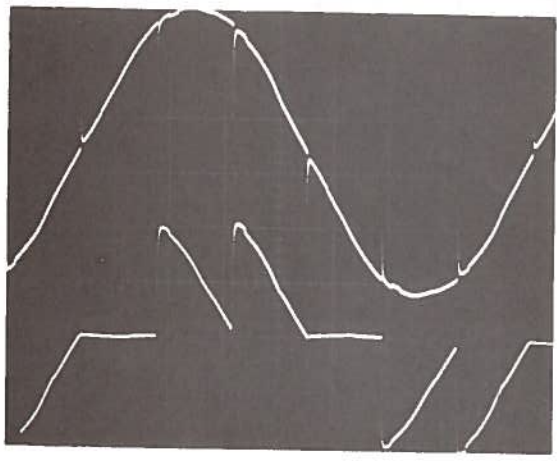

(d) .1Ω

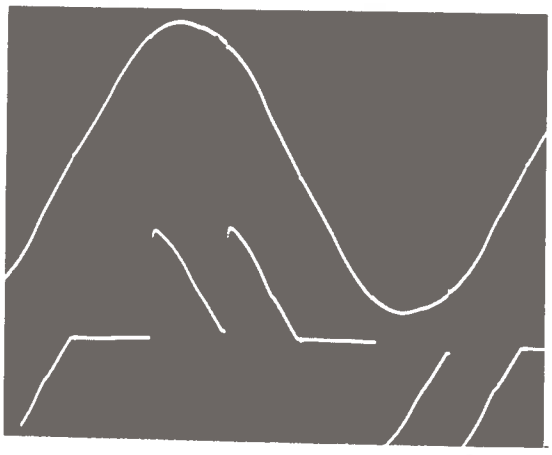

(e) 0Ω

Figure 4-12. Voltage and Current Variations Due to Line Reactance

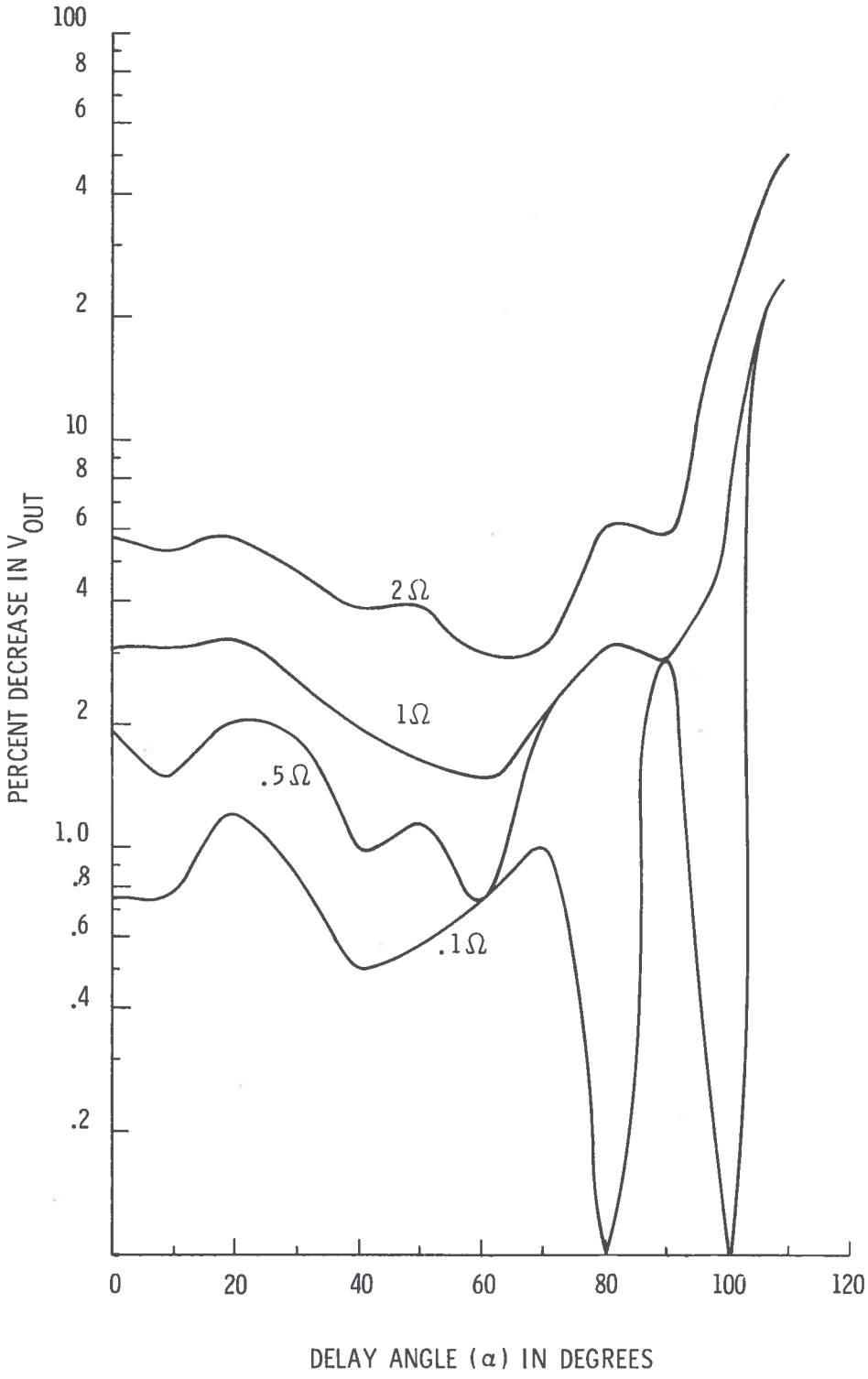

Figure 4-13. Percent Decrease in V_{out} vs Delay Angle

Figure 4-13 is a plot of the percent decrease in output voltage vs α for these configurations. Table 4-3 also lists the percent drop in output voltage for several reactance values including those illustrated.

TABLE 4-3 OUTPUT VOLTAGE DEPENDENCE ON SERIES LINE REACTANCE

DELAY ANGLE α (degrees)	V_{out}								
	X_L					Percent E_{out} Lost			
	0	0.1	0.5	1.0	2.0	0.1	0.5	1.0	2.0
110	4	3	3	2.5	2	25	25	37.5	50
100	15	15	14	14	12	0	6.7	6.7	20
90	35	34	34	34	33	2.75	2.75	2.75	5.7
80	64	64	62	62	60	0	3.1	3.1	6.2
70	98	97	96	96	95	1.02	2.04	2.04	3.06
60	136	135	135	134	132	.74	.74	1.48	2.96
50	174	173	172	171	167	.57	1.15	1.72	4.02
40	206	205	204	202	198	.495	.97	1.94	3.88
30	232	230	228	226	221	.86	1.72	2.58	4.72
20	250	247	245	242	236	1.2	2.00	3.20	5.6
10	260	258	256	252	246	.77	1.5	3.08	5.36
0	264	262	259	256	249	.758	1.89	3.03	5.67

The high inductance cases in Figure 4-12 represent extreme cases which would not exist in operational systems. They are included to demonstrate the degree to which series line reactance can influence performance. Since the losses in series reactance occur in the distribution system before the collection point, it is important to note that the input voltage to any other systems using the three-phase source would have the same distortion.

5. REACTIVE LOAD OPERATION

The preceding section presented a comparison between the measured and calculated characteristics of the PDR operating into an unfiltered resistive load. For the transit or traction applications, the typical load will include inductive filtering, either as a current smoothing reactor or as the magnetizing inductance of the motor itself.

Filtering not only purifies the DC output by smoothing the current, but also adds protection by preventing high current transients. The amount of filtering and type of filters used will depend on the application, the volume and weight allowance, source purity, etc. Inductance will be included in most systems because of the necessity for current transient control and ripple reduction.

The following sections present the results of laboratory measurements of a PDR operating with an inductively filtered load.

5.1 EFFECT OF INDUCTANCE

The addition of inductance to the output of the PDR modifies its characteristics from those of the unfiltered case. With an unfiltered resistance, load power flows to the load directly from the source and there is no energy stored during the cycle. When inductance is added, energy is stored in its magnetic field as load current increases, and is delivered to the load as current decreases. The inductor acts to stabilize the DC load current and smooth the ripple. When the per unit inductance is much higher than the resistance, the load will approach a ripple-free direct current for delay angles approaching 90°. At delay angles greater than 90°, where the conduction period of each thyristor would be less than 30°, inductive energy storage in series with the load cannot maintain continuous current. At these angles, the average output voltage would be negative and would require power flow from the load back to the source. This is an operational mode which is excluded from this study.

The PDR with inductive filtering in the load has three regions of operation, depending on the intensity of the load. First is the lightly loaded case, where the PDR will exhibit characteristics similar to those of the unfiltered case discussed earlier. Second is the case of a heavily loaded PDR, or constant current load, which can transfer power in either direction. For this case, the output current waveform will be essentially ripple free for all delay angles. Finally is the intermediate case, that is, with finite inductive filtering and an intermediate load. This was the case studied in the laboratory.

For an unfiltered resistive load, the output voltage and current waveforms are the same, and are in phase. Laboratory measurements of various characteristics are easily verified by analytical means. As the load becomes complex, due either to the addition of reactive energy storage for output filtering or to the reactive nature of typical traction loads, the mathematical computations become cumbersome. Not only are there differences in waveshapes and phase angle, but the magnitudes of these differences are dependent upon the ratio of the real to reactive impedance. The analytical derivation of the PDR characteristics for these complex loads is beyond the scope of this report. The measured characteristics for the resistive load have been compared to the calculated values and the measurement techniques verified. These same measurement techniques have been employed to determine the characteristics of the PDR operating into a reactive load.

Laboratory tests were conducted for several inductance to resistance ($L/_R$) ratios, and the results are presented in the following sections. The loading conditions under which the tests were conducted included the unfiltered resistance (L=0) case, although it had been covered in depth earlier. It is included here for comparison purposes.

The PDR operating with constant current is the operational mode analyzed in most documents and textbooks. This mode of operation assumes that the energy stored in the inductor is large enough to maintain a constant current. For many applications the ripple is so low that this is a reasonable assumption. Another

assumption for this mode of operation is that the load voltage is a DC value equivalent to the average output voltage, such as a battery or the back EMF of a DC motor. This particular operational mode is easily handled analytically because formulae for output voltage, power and power factor, at all delay angles, are proportional to the cosine of the phase angle. With an assumed constant current, the thyristor conduction interval is always 120° and the harmonic distortion is at its minimum. Although the assumption of infinite inductance, hence constant current, simplifies the analysis of the PDR, it does not provide insight into the operation with either passive loads or lightly loaded machines.

Figure 5-1 shows the effect of inductance on voltage and current waveforms for different values of delay angle. For the load current to be a pure DC, either the resistance must be zero or the inductance infinite. Since neither condition is possible, some ripple current through the load is inevitable. Note that the load current pulses do not have abrupt transitions and that thyristor conduction intervals are longer. At delay angles above 90°, the thyristor conduction periods do not overlap, they commutate when the current drops to zero. The output voltage polarity goes negative when the inductor magnetic field begins to collapse, but the thyristors are forward biased because of the induced voltage in the inductor. The average output voltage is positive even though there is a negative voltage for a portion of the cycle. As the phase delay angle is decreased further, the conduction periods of the thyristors overlap and the stored inductor energy is never completely dissipated.

Table 5-1 lists the measured values of output voltage, line current, power, apparent power, and power factor as a function of delay angle for several inductance to resistance ratios. The conditions of resistance only without filtering (L=0), and constant current (L=∞) are also included. The values of inductance chosen for the laboratory measurements were 0.5, 1.0, and 2.0 per unit, using a 60 Hz impedance of 30Ω as a base. The normalized values of the parameters listed in Table 5-1 are listed in Table 5-2, and these normalized values are used in the various figures.

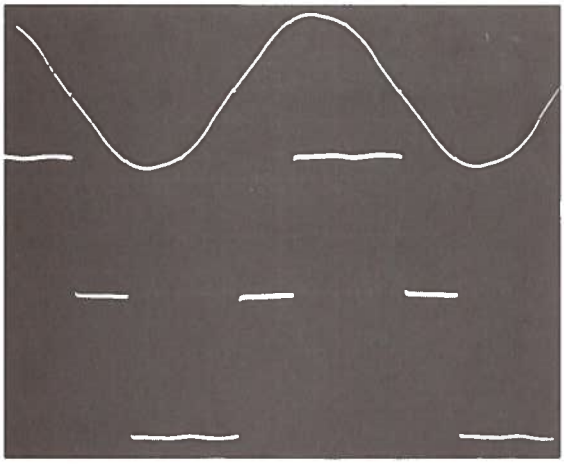

(a) $\alpha = 0^{\circ}$

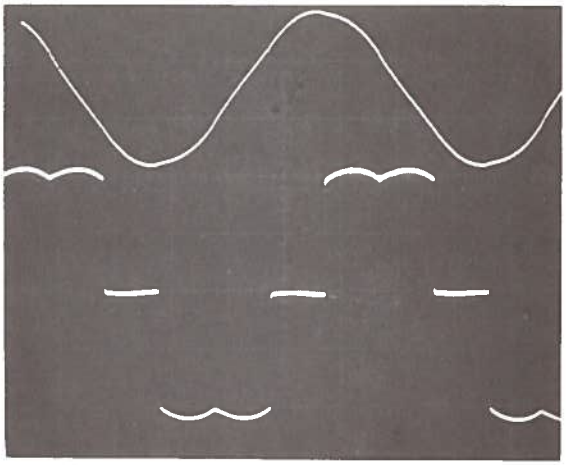

(b) $\alpha = 30^{\circ}$

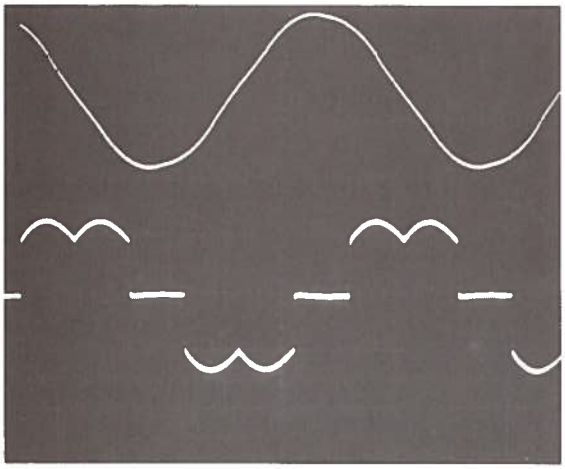

(c) $\alpha = 60^{\circ}$

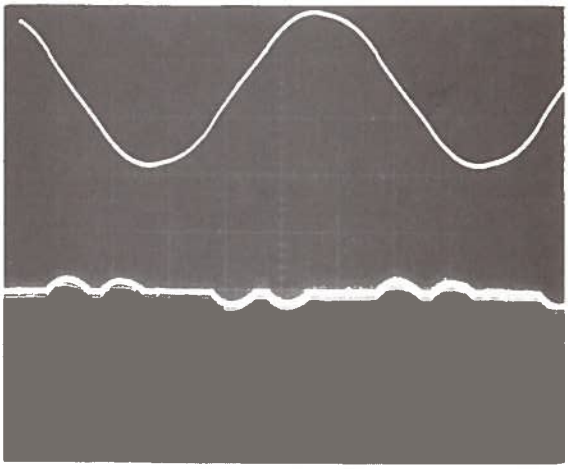

(d) $\alpha = 90^{\circ}$

Figure 5-1. Smoothing Inductor and Resistive Load

TABLE 5-1 MEASURED VALUES FOR VARIOUS $\frac{L}{R}$ RATIOS

α (degrees)	1 OUTPUT VOLTAGE				2 I_{RMS}				3 P				4 S_T			
	2.0	1.0	0.5	0	2.0*	1.0	0.5	0	2.0*	1.0	0.5	0	2.0*	1.0	0.5	0
120	0	0	0	0	0	0	0	0	0	0	0	0	0	0	0	0
110	0	0	2	4	.127	.060	.160	.192	-	0	0	10	-	22	56.1	70
100	3	5	11	15	.415	.160	.2560	.660	-	-	4	24	44	55	89.6	230
90	10	17	28	34	1.970	.384	.0705	1.310	4	10	36	96	143	130	247	457
80	43	47	52	62	4.030	1.090	1.280	2.080	126	76	114	236	682	377	448	725
70	86	93	102	96	6.150	2.210	2.430	2.880	464	276	340	458	1384	760	850	1000
60	129	133	143	135	7.970	3.140	3.380	3.710	1016	546	640	738	2110	1080	1180	1300
50	167	172	180	176		4.030	4.280	4.520	1680	884	1006	1070	2736	1390	1500	1580
40		245	213	209		4.870	5.070	5.240		1266	1382	1424		1680	1780	1820
30		230	237	234		5.470	5.620	5.740		1592	1704	1704		1890	1970	1990
20		248	254	252		5.930	6.070	6.140		1852	1952	1950		2040	2130	2140
10		259	265	264		6.170	6.300	6.330		2001	2118	2114		2120	2200	2210
0		263	268	267		6.210	6.370	6.400		2064	2154	2164		2140	2230	2230

*$\frac{L}{R}$ = 2.0pu L = 1.0pu R = 0.5pu

TABLE 5-2 NORMALIZED RECORDED VALUES FOR VARIOUS $\frac{L}{R}$ RATIOS

α (degrees)	1 OUTPUT VOLTAGE L=∞	2pu	1pu	0.5pu	0pu	2 LINE CURRENT L=∞	2	1	0.5	0	3 POWER L=∞	2	1	.5	0
110	-	0	.003	.007	.014	-	0	0	0	.030		0	0	0	.004
100	-	.011	.022	.033	.055	-	.010	.015	.03	.105		0	0	.002	.011
90	0	.037	.065	.091	.132	0	.034	.060	.098	.204	0	.001	.004	.016	.043
80	.173	.160	.098	.179	.228	.173	.162	.182	.182	.325	.028	.029	.035	.052	.105
70	.342	.321	.345	.342	.353	.342	.332	.341	.341	.450	.105	.106	.127	.150	.204
60	.500	.482	.507	.507	.497	.500	.507	.500	.515	.579	.240	.234	.251	.282	.328
50	.642	.623	.646	.647	.646	.642	.657	.651	.652	.705	.390	.385	.406	.467	.476
40	.766		.772	.772	.770	.766		.788	.788	.820	.550		.581	.610	.633
30	.866		.866	.864	.862	.866		.884	.887	.893	.712		.730	.752	.758
20	.940		.935	.932	.927	.940		.955	.955	.960	.880		.850	.862	.867
10	.984		.975	.975	.972	.984		.985	.985	.987	.920		.920	.935	.940
0	1.000		.990	.990	.980	1.000		1.000	1.000	1.000	.950		.950	.95	.965

α (degrees)	4 APPARENT POWER L=∞	2	1	.5	0	5 REACTIVE POWER L=∞	2	1	.5	0	6 POWER FACTOR L=∞	2	1	.5	0
110	-	0	0	.025	.020	-	0	0	.025	.031		-	0	0	0
100	-	.010	.015	.041	.093	-	.10	.015	.040	.105		-	.056	.020	.110
90	0	.034	.061	.111	.201	0	.034	.061	.110	.201	0	.03	.057	.080	.222
80	.173	.161	.181	.215	.328	.163	.158	.177	.193	.307	.165	.186	.188	.230	.356
70	.342	.327	.340	.381	.460	.309	.305	.316	.349	.398	.327	.335	.360	.370	.448
60	.500	.500	.501	.529	.580	.419	.437	.431	.447	.480	.478	.482	.560	.514	.555
50	.642	.645	.667	.672	.680	.485	.512	.513	.499	.525	.614	.612	.615	.636	.682
40	.766		.788	.797	.806	.499		.512	.503	.570	.732		.740	.745	.762
30	.866		.885	.884	.895	.465		.464	.442	.456	.827		.820	.838	.837
20	.940		.955	.955	.954	.395		.395	.387	.398	.898		.885	.890	.890
10	.985		.982	.987	.985	.321		.308	.266	.259	.940		.935	.938	.933
0	1.000		1.000	1.000	1.000	.283		.255	.259	.243	.955		.950	.948	.940

5.2 OUTPUT VOLTAGE

The output voltage as a function of delay angle for several per unit reactance to resistance ratios are listed in Table 5-1, column 1. Normalized values are listed in Table 5-2, column 1, and plotted in Figure 5-2. For those cases where the thyristor conduction interval is 120° per cycle, the expression for output voltage is:

$$E_d = E_{do} \cos \alpha$$

For the constant current case, the current does not fall to zero and the thyristor conduction interval is 120° for all delay angles. At the other extreme, when there is no inductive filtering, the thyristors commutated at $\alpha = 60°$.

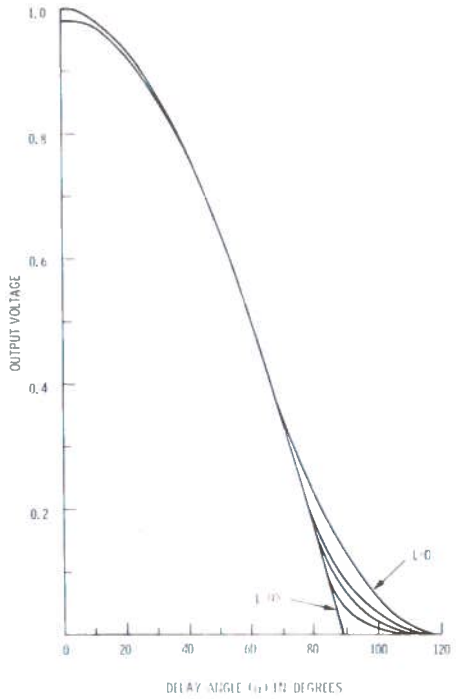

Figure 5-2. Output Voltage vs Delay Angle for Various Inductance Values

The difference between the two cases is a result of the induced voltage in the reactance. During the interval that load power is supplied by the collapsing magnetic field, the output voltage is negative. This negative voltage contributes to, and lowers, the average output voltage. As the per unit reactance is increased, the stored energy and thyristor conduction intervals also increase. The result is a family of curves which are co-linear to $\alpha = 60°$. They diverge from the constant current curve at the delay angles at which the current becomes discontinuous. The point at which each curve separates is a function of the reactance to resistance ratio as shown in Figure 5-2.

5.3 LINE CURRENT

Values for RMS line current as a function of delay angle for several per unit reactance to resistance ratios are listed in Table 5-1, column 2. The normalized values are listed in Table 5-2, column 2, and plotted in Figure 5-3.

For the constant current case, we have assumed a fixed load with infinite inductance, such that the load current is ripple-free but of a magnitude proportional to the average output voltage:

$$I_d = \frac{E_d}{R} = \frac{E_{do}}{R} \cos \alpha$$

The RMS line current has fundamental and harmonic components. As the per unit reactance is increased from zero to infinity, the impedance to all of the frequency components increases and a lower current for a given voltage results. The plot shows that the magnitude of the reactance to resistance ratio becomes significant only at the higher delay angles where the magnitudes of the harmonics are high.

5.4 POWER

The power dissipated in the load as a function of the delay angle is listed in Table 5-1, column 3. Normalized values are listed in Table 5-2, column 3, and plotted in Figure 5-4.

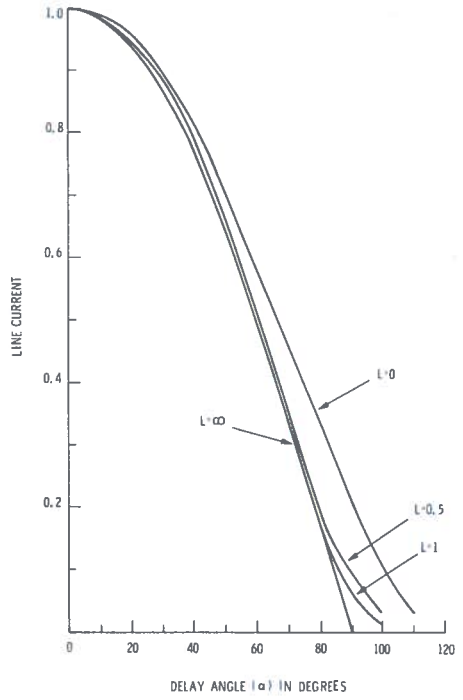

Figure 5-3. Line Current vs Delay Angle for Various Inductance Values

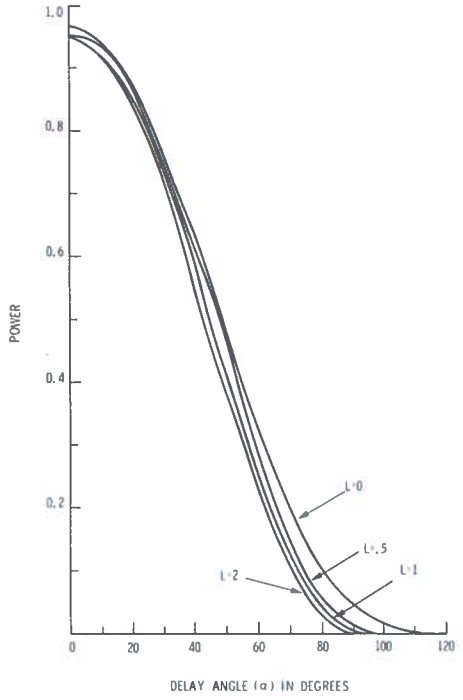

Figure 5-4. Power vs Delay Angle for Various Inductance Values

5.5 APPARENT POWER

The total apparent power vs delay angle for the inductively filtered load is listed in Table 5-1, column 4. The normalized values are listed in Table 5-2, column 4, and plotted in Figure 5-5.

5.6 REACTIVE POWER

The total reactive power, distortion reactive power and displacement reactive power were measured using the techniques described in the section on power measurements. These components are listed in Table 5-2, column 5, and plotted in Figure 5-6.

The series combination of resistance and inductance is a frequency-dependent impedance which increases as the filter inductance increases, thus causing a reduction in current magnitude for each delay angle. The frequency dependence of the load impedance results in phase and magnitude differences for both the fundamental and the harmonics. These phase effects are primarily manifested as increased displacement angles between the fundamental voltage and current components. They add to the displacement component of reactive power and a lower phase displacement power factor. The impedance presented to each of the harmonic components of current, however, is increased by a factor equal to the order number of the harmonic, and thus the total distortion component of reactive power and the output ripple are reduced significantly. At delay angles where the current is discontinuous, the higher impedance of the inductor limits the rate of current change and produces smooth current pulses.

5.7 POWER FACTOR

The system power factors for the inductively filtered load configurations are listed in Table 5-2, column 6, and plotted in Figure 5-7.

The measured power factor with inductance filtering is lower than that measured with the resistance-only load. The inductance presents a high impedance to the harmonics, thus the harmonics

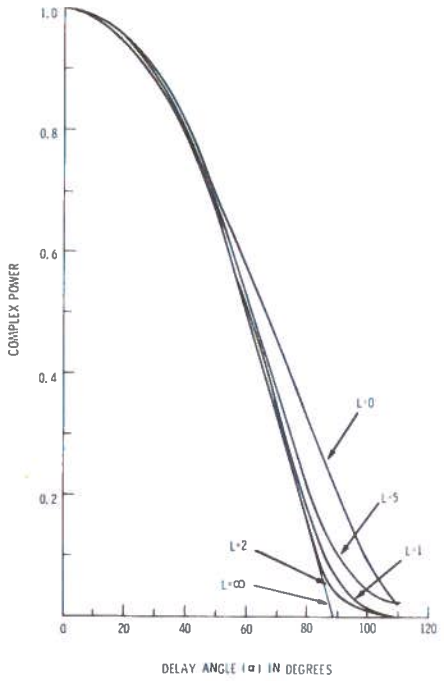

Figure 5-5. Complex Power vs Delay Angle

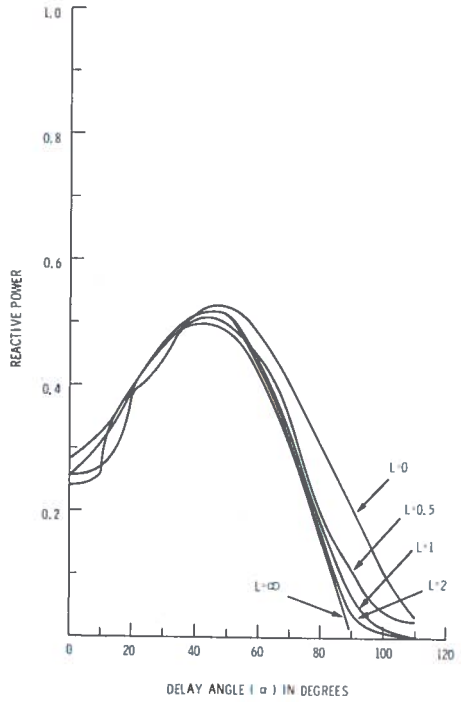

Figure 5-6. Reactive Power vs Delay Angle for Various Inductive Loads

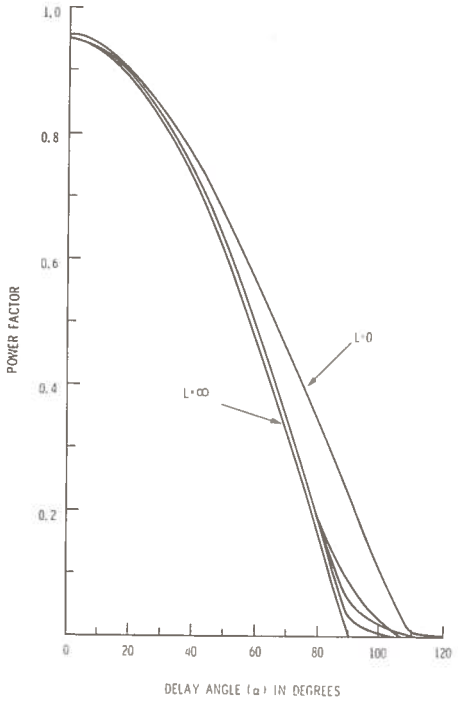

Figure 5-7. Power Factor vs Delay Angle for Various Values of Inductance

(and hence distortion power) are reduced. The inductance, however, introduces additional phase displacement between the fundamental components of voltage and current. The displacement power factor and total power factor are thus reduced. The reductions in output ripple, however, warrant the decrease in system power factor.

5.8 HARMONICS

In a system such as the PDR, where the line current waveform is chopped, harmonic components of current will be generated. The magnitudes of these harmonics can be minimized by adding inductive filters to the output. With infinite inductance, the minimum amplitude of each harmonic is achieved. At this point, the magnitude of the harmonic current is inversely proportional to its order. That is:

$$I_n = \frac{1}{n} I_1$$

TABLE 5-3 HARMONIC CURRENTS FOR REACTIVE LOAD CASE

α	I_5/I_1					I_7/I_1				
	L=∞	2	1	.5	0	L=∞	2	1	.5	0
110	.2	-	-	.800	-	.140	-	-	.770	-
100	.2	.800	.830	.760	.850	.140	.630	.580	.640	.750
90	.2	.570	.680	.650	.815	.140	.270	.310	.390	.650
80	.2	.280	.320	.470	.700	.140	.040	.080	.170	.500
70	.2	.250	.280	.350	.630	.140	.080	.050	.060	.380
60	.2	.230	.260	.290	.500	.140	.110	.080	.040	.250
50	.2	.220	.230	.270	.380	.140	.120	.100	.065	.170
40	.2		.220	.270	.320	.140		.115	.105	.126
30	.2		.217	.240	.260	.140		.112	.110	.125
20	.2		.210	.210	.240	.140		.127	.120	.120
10	.2		.200	.206	.220	.140		.129	.130	.120
0	.2		.200	.200	.220	.140		.133	.130	.115

	I_{11}/I_1					I_{13}/I_1				
	L=∞	2	1	.5	0	L=∞	2	1	.5	0
110	.0909	-	-	.500	-	.077	-	-	.500	-
100	.0909	.230	.250	.270	.600	.077	.080	.080	.120	.500
90	.0909	.070	.060	.020	.420	.077	.080	.080	.100	.280
80	.0909	.080	.070	.100	.230	.077	.030	.040	.060	.230
70	.0909	.080	.070	.090	.220	.077	.050	.040	.010	.200
60	.0909	.090	.085	.090	.180	.077	.060	.050	.030	.180
50	.0909	.095	.092	.090	.170	.077	.063	.050	.040	.110
40	.0909		.093	.100	.126	.077		.060	.080	.070
30	.0909		.010	.090	.100	.077		.075	.070	.070
20	.0909		.093	.090	.090	.077		.072	.065	.060
10	.0909		.088	.087	.100	.077		.068	.067	.060
0	.0909			.085	.087	.077		.071	.070	.060

where n is the order of the harmonic. However, in the laboratory experiments where finite values of inductance and resistance were used, the magnitude of each of these harmonics increased from this 1/n value as the per unit inductance decreased to zero.

The experiments conducted included measurements of the harmonic currents. The data for the 5th, 7th, 11th, and 13th are presented here in Table 5-3. The higher harmonics exhibit the same characteristic. In the succeeding graphs, Figures 5-8 to 5-11 are plotted for the different values of filter inductance. These graphs show how the magnitude of the harmonics approaches I_1/n at greater delay angles as the inductance is increased.

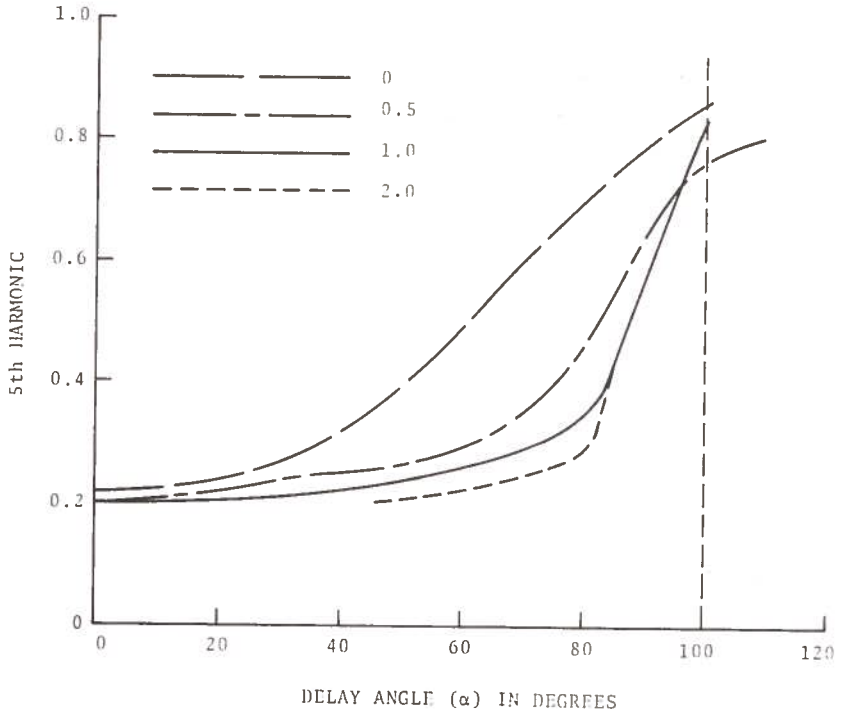

Figure 5-8. 5th Harmonic vs Delay Angle for Various Inductance Values

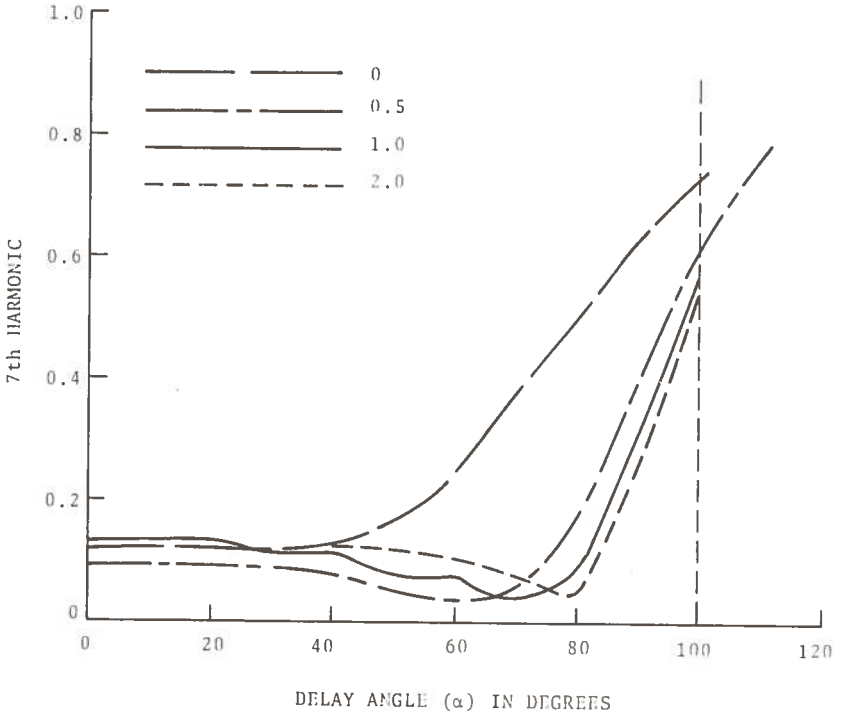

Figure 5-9. 7th Harmonic vs Delay Angle for Various Inductance Values

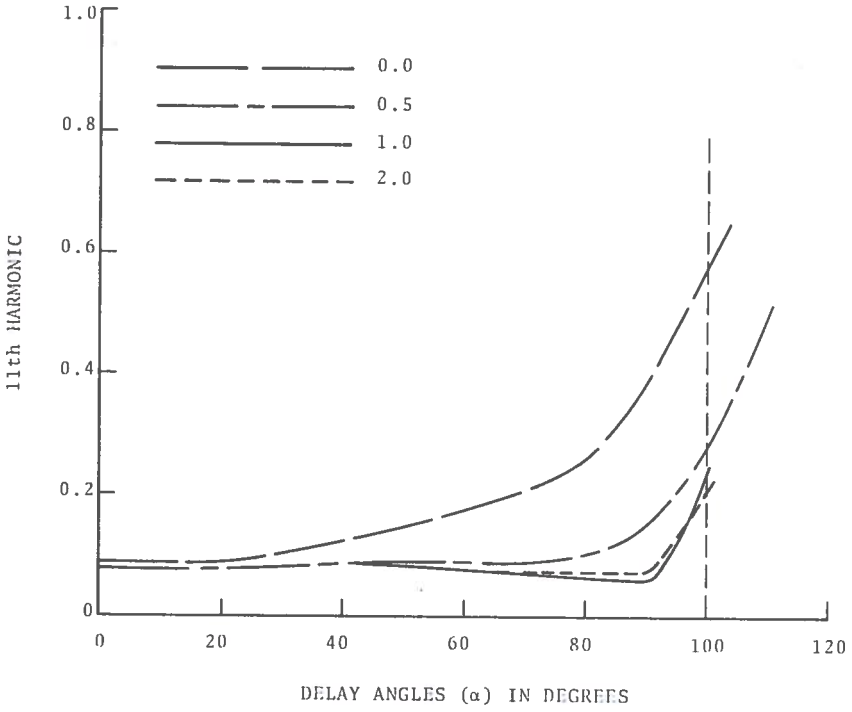

Figure 5-10. 11th Harmonic vs Delay Angle for Various Inductance Values

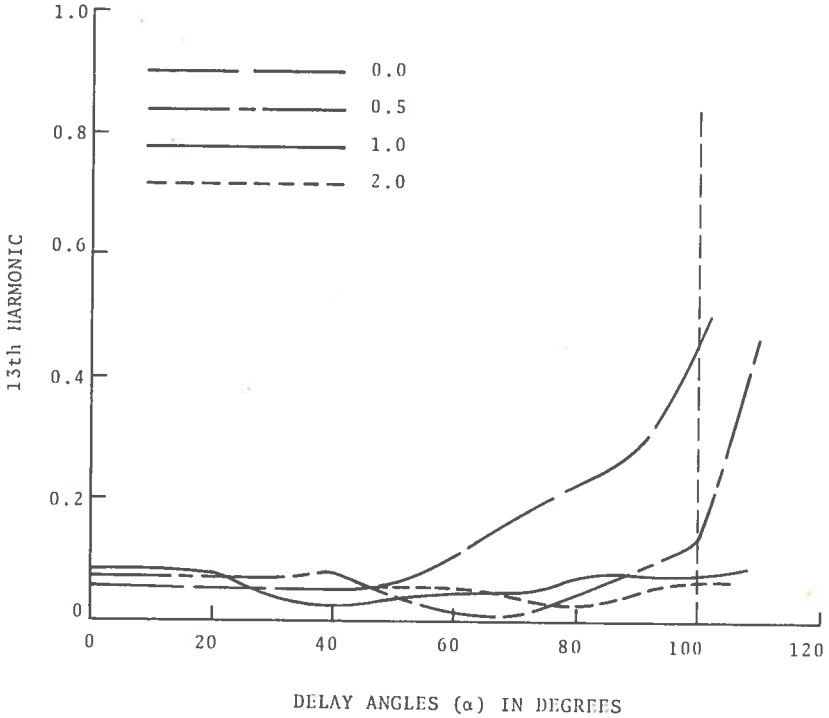

Figure 5-11. 13th Harmonic vs Delay Angle for Various Inductance Values

6. FREE-WHEELING DIODE

There are two methods of handling the current generated by the collapse of the inductor magnetic field. The first of these, described earlier, allows the voltage induced in the inductance to hold the thyristors on and extend their conduction interval until the energy stored in the magnetic field is dissipated. The second uses a diode connected in the reverse direction across the PDR output. The diode becomes forward biased when the line to line voltage reverses. This by-pass diode is called a "free wheeling diode" (D1 in Figure 2-1). The operation of the free wheeling diode (FWD) is as follows. The collapse of the magnetic field induces a voltage which maintains the current flow in the load. Without the free wheeling diode, this voltage would forward bias the power thyristors and extend their conduction interval. However, the FWD clamps the output voltage and allows the power thyristors to commutate. The reactive current thus flows through the free wheeling diode and not through the power lines. All of the energy stored in the inductor is constrained to be dissipated in the load and none of it is returned to the source. For a given delay angle where the FWD is operational ($\alpha>60°$), the parameters are higher than with only inductive filtering.

The FWD is operational only for delay angles of 60° or greater, since at lower delay angles the thyristor conduction periods overlap and the diode is never forward biased. The effects of the FWD on the circuit can be seen in Figure 6-1. Figure 6-1a shows the voltage at the output of the PDR, without the free wheeling diode. The output voltage goes negative when the line to line voltage goes negative because of the induced voltage in the inductance. With the FWD (Figure 6-1b) the output voltage is clamped at zero and the reactive current passes through it.

Because the FWD does not allow reactive current to pass back to the source and also does not allow the output of the PDR to reverse polarity, the use of the FWD limits the PDR to single quadrant, this is, rectifier operation.

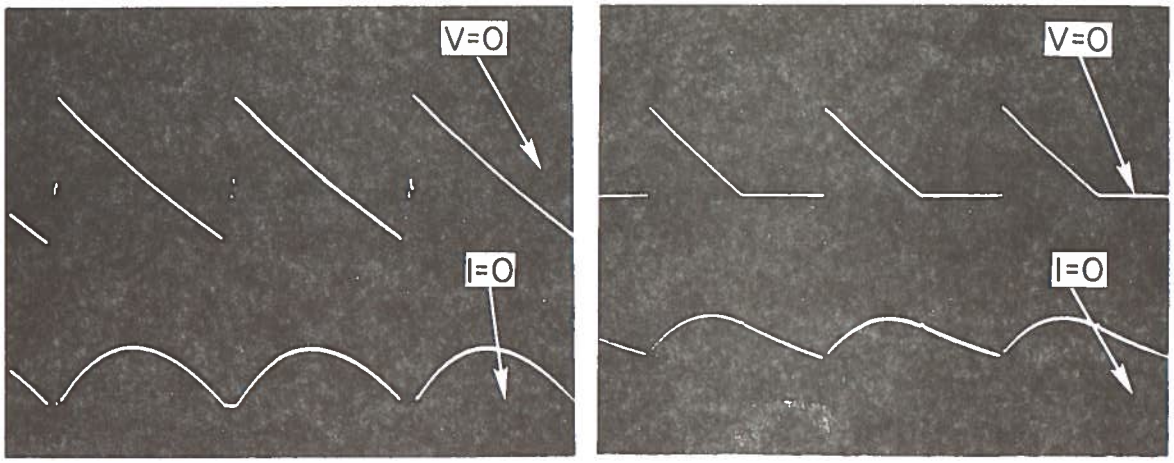

(a) R and L without FWD (b) R and L with FWD

Figure 6-1. Output Voltage and Load Current for $\alpha = 60°$

Comparison of Figure 4-1 with Figure 6-2 shows that below $\alpha = 60°$ the FWD has no effect on circuit performance. As α is increased from 60° to 120°, the FWD bypasses the reactive current and clamps the voltage to zero. The current decays exponentially toward zero with a time constant of L/R seconds.

The voltage across the inductor for the two cases is shown in Figure 6-1. The top trace shows that without the FWD the inductor voltage induced by the collapse of the magnetic is higher than with the free wheeling diode. The voltage across the inductor is equal to the sum of the line to line voltage and the drop across the resistance in one case, and to the drop across the resistance in the other case. The lower trace shows that the clamping action of the FWD maintains a lower voltage differential across the inductor. The voltage across the inductor is given by:

$$e = L \frac{d_i}{dt}$$

TABLE 6-1 RECORDED AND NORMALIZED VALUES FOR PDR WITH FREE-WHEELING DIODE

α	E_{OUT} RECORDED Volts	E_{OUT} NORMALIZED $E_o/268$	I_{RMS} RECORDED	I_{RMS} NORMALIZED $I_{RMS}/2.06$	POWER RECORDED	POWER NORMALIZED	REACTIVE POWER RECORDED	REACTIVE POWER NORMALIZED	APPARENT POWER RECORDED	APPARENT POWER NORMALIZED	POWER FACTOR RECORDED	I_H I_5/I_1	I_H I_7/I_1	I_H I_{11}/I_1	I_H I_{13}/I_1
115	1.0	0	.0005	-	0	0	0	0	0	0					
110	4.0	.015	.010	.005	0	0	22.5	.021	22.50	.019		1.250	1.500	1.250	1.000
105	8.0	.030	.030	.014											
100	15.0	.056	.070	.033	10	.0043	66.8	.062	67.50	.058	.148	.930	.830	.560	.420
95	22.0	.082	.120	.058											
90	35.0	.131	.205	.100	38	.0170	225.0	.202	225.0	.190	.167	.770	.560	.140	.060
85	48.0	.179	.300	.145											
80	65.0	.243	.430	.209	134	.0590	433.0	.397	450.0	.372	.298	.590	.290	.110	.180
75	82.0	.306	.560	.272											
70	101.0	.377	.720	.350	304	.1340	706.0	.648	768.0	.605	.397	.410	.060	.160	.080
65	119.5	.446	.880	.427											
60	138.0	.515	1.050	.514	614	.2720	997.0	.915	1170.0	.857	.507	.250	.077	.085	.043
50	177.0	.660	1.360	.660											
40	210.0	.783	1.615	.784											
30	236.0	.880	1.815	.882											
20	253.0	.940	1.940	.940											
10	264.0	.985	2.020	.980											
0	268.0	1.000	2.040	.990											

The voltage across the inductor remains lower with the FWD in place, therefore the change in current is lower and there is less energy per cycle taken from the inductor. The exponential decay of current with a high time constant also results in a high output current with less ripple.

Table 6-1 lists the recorded and normalized parameters for the PDR operating with a free wheeling diode. These parameters are plotted in Figures 6-2 to 6-8. The effect of the free wheeling diode will become more evident in the next section.

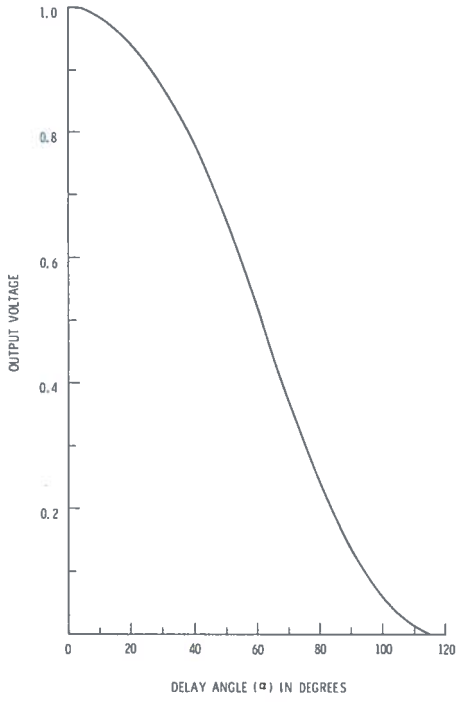

Figure 6-2. Output Voltage vs Delay Angle for Operation with FWD

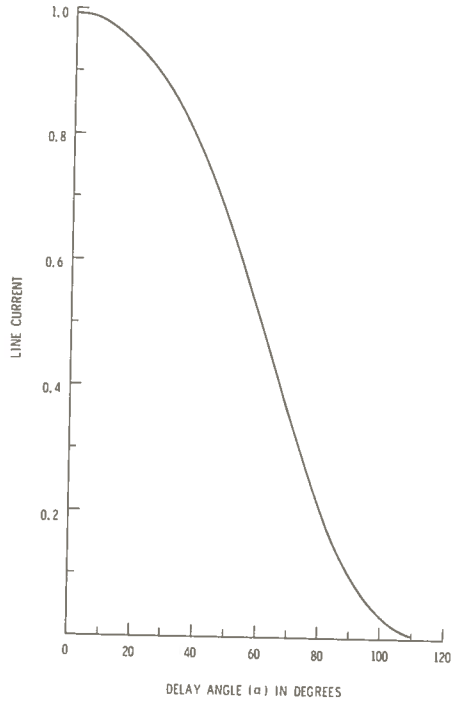

Figure 6-3. Line Current vs Delay Angle for Operation with FWD

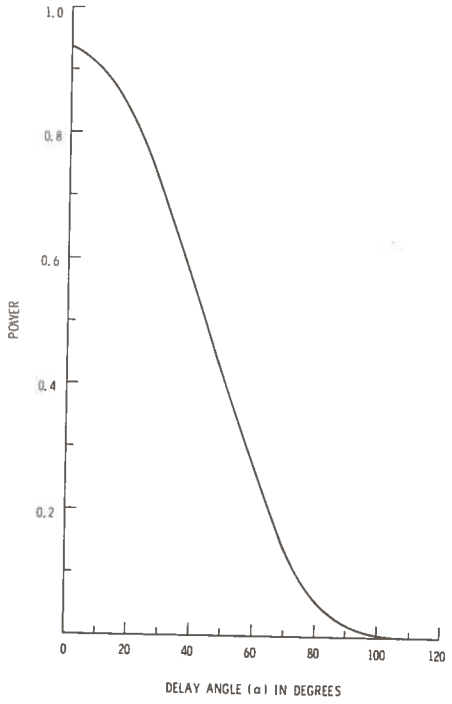

Figure 6-4. Power vs Delay Angle for Operation with FWD

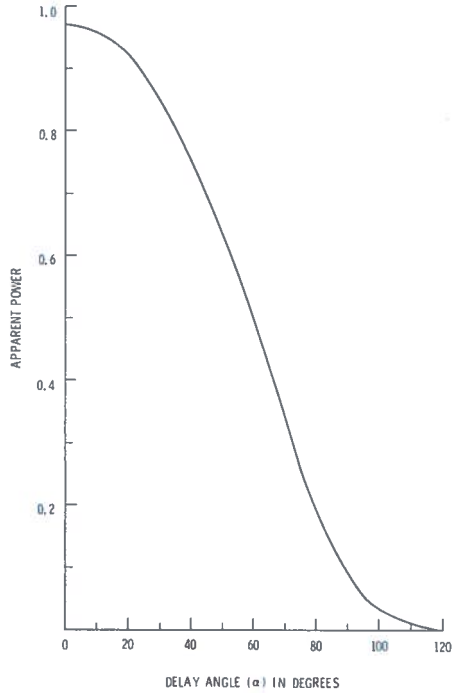

Figure 6-5. Apparent Power vs Delay Angle for Operation with FWD

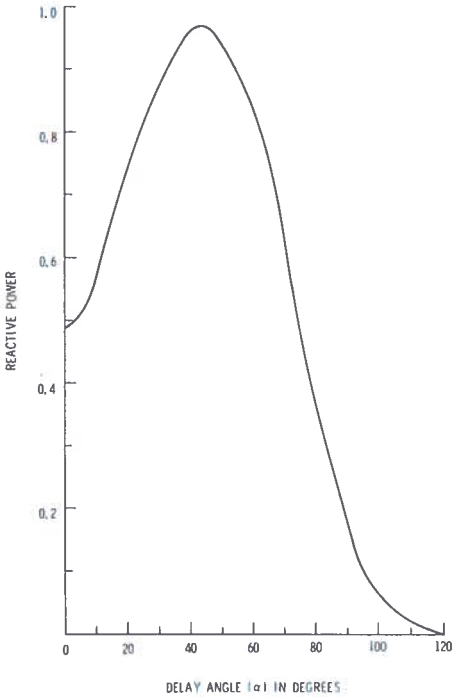

Figure 6-6. Reactive Power vs Delay Angle for Operation with FWD

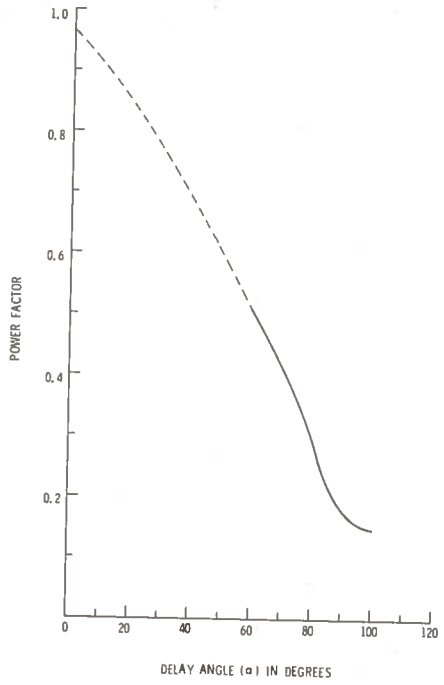

Figure 6-7. Power Factor vs Delay Angle for Operation with FWD

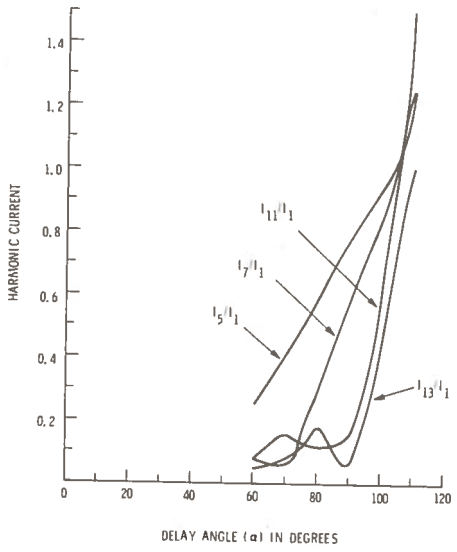

Figure 6-8. Harmonic Currents vs Delay Angle for Operation with FWD

7. COMPARISON OF EFFECTS OF DIFFERENT LOADS

The different characteristics exhibited by the PDR for various loads have been presented and discussed in the previous sections. Each of the different parameters will now be discussed in terms of comparing the effects of the various load conditions: resistive, inductive, and inductive with a free wheeling diode.

7.1 OUTPUT VOLTAGE

Since the FWD prevents the output voltage from going negative, the resultant waveform is the same as for the resistive load case. Therefore, the output voltage for all delay angles is the same for either the resistive load or for the inductive load with a FWD. The output voltage for the inductive load without the FWD is lower than the other two cases, because the intervals where the voltage is negative serve to reduce the average voltage. The magnitude of this reduction is shown by the curves in Figure 7-1 for all delay angles.

7.2 LINE CURRENT

The line current curves shown in Figure 7-2 are lower for the two cases of inductive filtering. This is due to the increase in the impedance of the load, and to the filtering of the harmonics.

The FWD which bypasses current during part of the cycle, introduces additional discontinuities into the line current waveform. This results in increased harmonic distortion and therefore RMS currents higher than for the case of the inductive load without the FWD.

7.3 POWER

The power delivered by the PDR for the three cases is shown in Figure 7-3. The curves for the two cases with inductive filtering are lower than the curve for the unfiltered case. This is so because, although the filtering smooths the waveforms, it also increases the impedance seen by the PDR and hence lowers the output

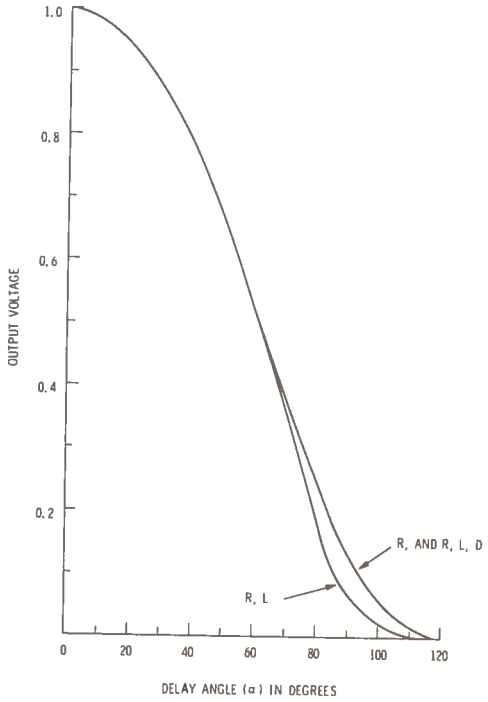

Figure 7-1. Comparison of Output Voltage for Three Load Cases

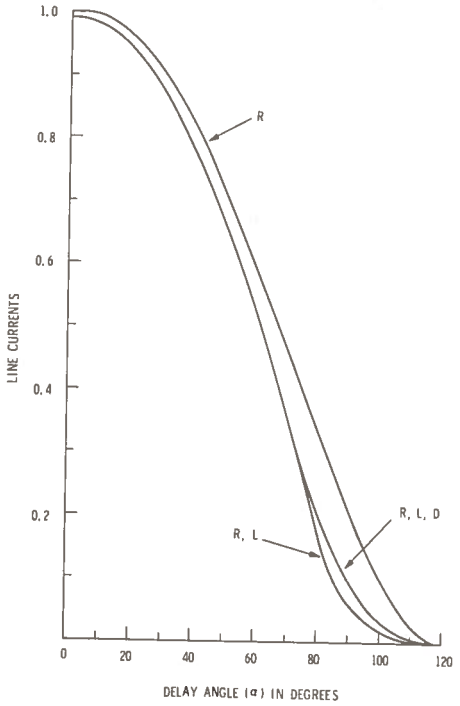

Figure 7-2. Comparison of Line Currents for Three Load Cases

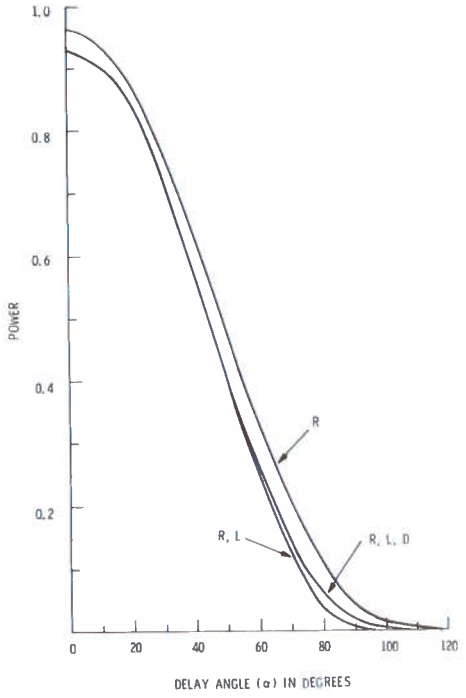

Figure 7-3. Comparison of Power for Three Load Cases

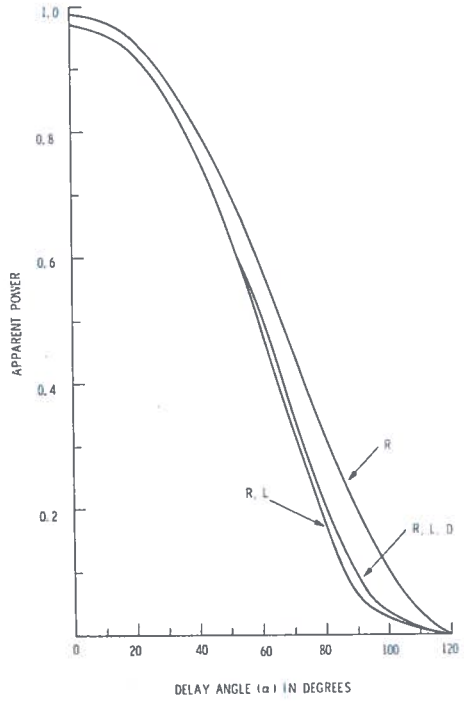

Figure 7-4. Comparison of Apparent Power for Three Load Cases

power. The inductive case with the FWD delivers more power than the case without the diode, for the same reason that the current is increased.

7.4 APPARENT POWER

The variation of apparent power delivered to the load for the three cases is shown in Figure 7-4. As expected, the effect of the different loads on the apparent power is the same as for the real power.

7.5 REACTIVE POWER

Reactive power as a function of delay angle for the three load cases is shown in Figure 7-5. The effect of inductance and free wheeling is the same as for the complex power and real power cases.

7.6 POWER FACTOR

The power factor variation for all three load cases is shown in Figure 7-6. The power factor for the two cases of inductive load is lower than for the resistive load because of the inductive effect in the curcuits. Although the smoothing effect (i.e., decreasing harmonics) of the inductor tends to increase the power factor, the current delay effect is greater, resulting in a lower overall power factor. With the FWD, the harmonic distortion is increased because of the additional current chopping and the reduction in phase angle between the fundamental current and voltage results in a higher displacement power factor.

7.7 HARMONICS

As should be expected, the effect of the different loads is the same for the harmonic currents as for the total RMS line current, the curves demonstrating this effect are shown in Figures 7-7, 7-8, 7-9, and 7-10.

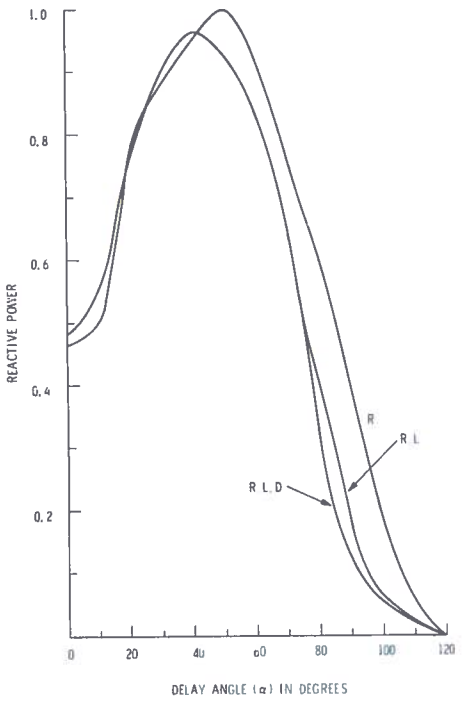

Figure 7-5. Comparison of Reactive Power for Three Load Cases

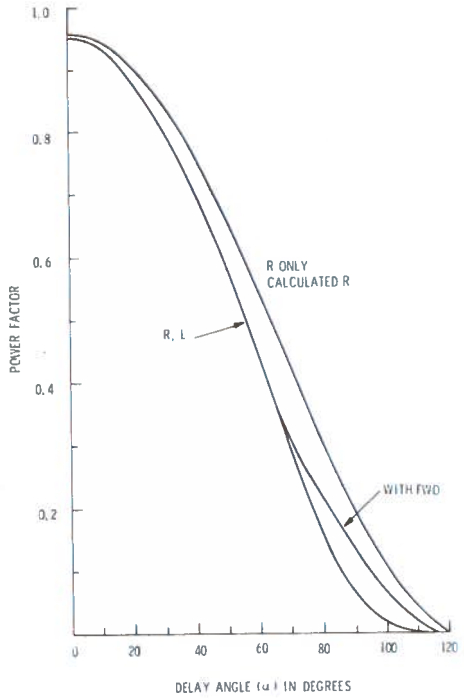

Figure 7-6. Comparison of Power Factor for Three Load Cases

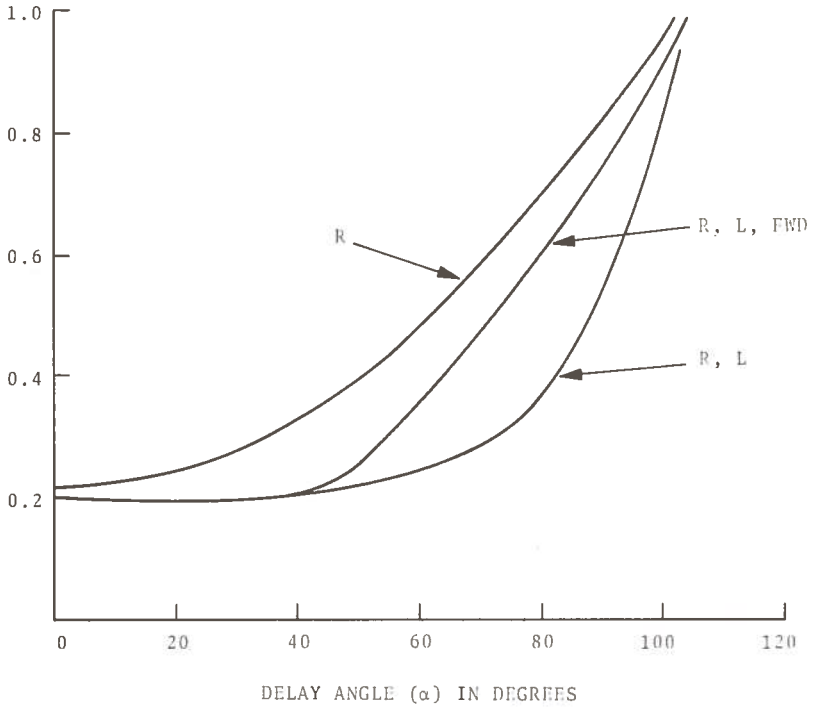

Figure 7-7. Comparison of 5th Harmonic for Three Load Cases

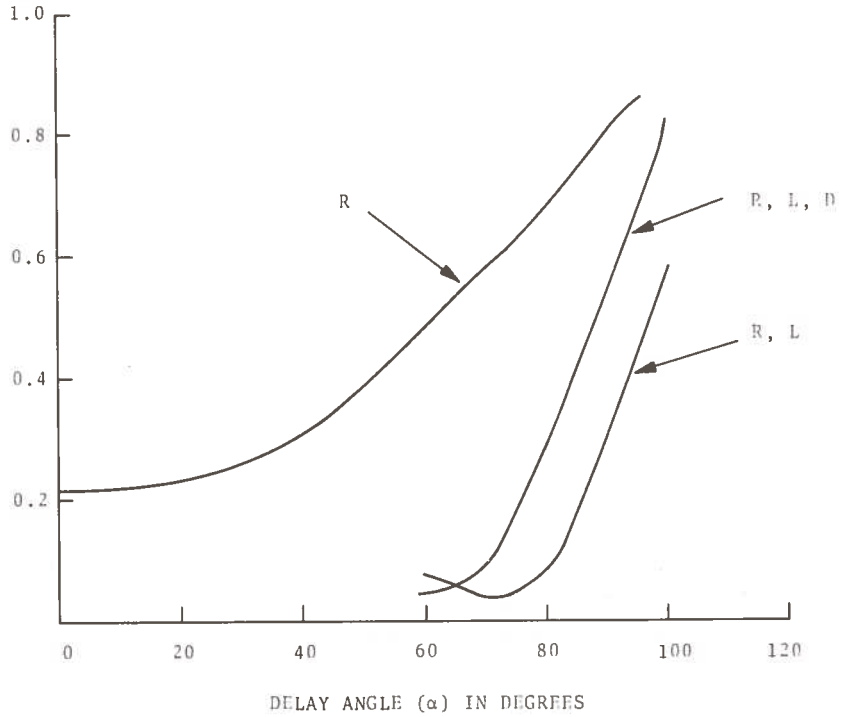

Figure 7-8. Comparison of 7th Harmonic for Three Load Cases

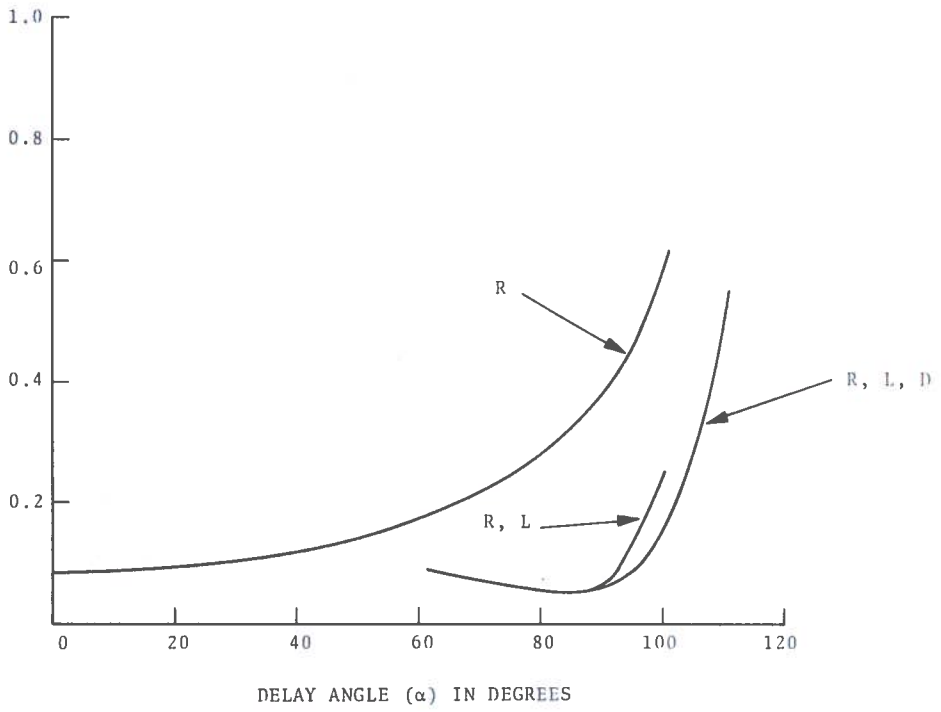

Figure 7-9. Comparison of 11th Harmonic for Three Load Cases

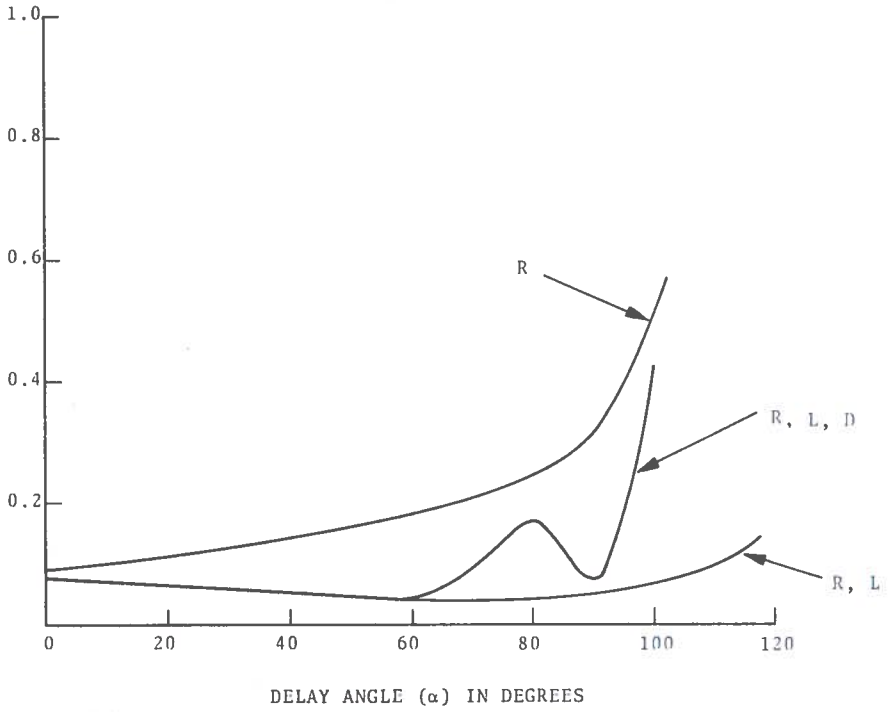

Figure 7-10. Comparison of 13th Harmonic for Three Load Cases

8. SUMMARY

The laboratory tests on the PDR have demonstrated the importance of proper equipment and techniques in measuring its total power characteristics. Conventional two-wattmeter methods of measuring reactive power are not accurate for determining the total reactive power. Attention must be given to the harmonic distortion when determining the total power characteristics of a system.

The effect of series line reactance was also considered. Although this reactance results in a decreased output voltage capability, its major effect is the increased distortion of the input voltage waveform. This could be a source of interference to the other systems operating from the same power supply.

A PDR will not typically operate into an unfiltered resistive load, however this is an operating condition which is most easily analyzed using analytical as well as experimental techniques. Analytically, all of the system's power characteristics can be expressed as a function of the phase control factor $f(\alpha)$. In this manner the experimental techniques can be validated with a high degree of confidence.

By adding inductance to this unfiltered resistive load, we can operate the PDR closer to expected typical operating conditions. The inductance has the effect of smoothing the output DC waveform, which lowers its harmonic content; however it also increases the phase displacement reactive power which decreases the total power factor. The addition of a FWD further reduces the ripple and improves the power factor, because the diode constrains the energy stored in the inductance to be dissipated only in the load. The deleterious effects of the FWD are increased harmonic distortion and incapability of bilateral operation.

9. BIBLIOGRAPHY

Bedford, B. D. and Hoft, R. G., Principles of Inverter Circuits, John Wiley and Sons, New York, 1964.

Kerchner, R. M. and Corcoran, G. F., Alternating Current Circuits, John Wiley and Sons, New York, 1962.

Shaefer, J., Rectifier Circuits: Theory and Design, John Wiley and Sons, New York, 1965.

APPENDIX
POWER SYSTEM MEASUREMENTS

A-1 MEASUREMENT OF SINUSOIDAL WAVEFORMS

The power flow in a three-phase system can be resolved into components according to the following criteria.

a) The apparent power is the total volt-ampere power which flows into the system. It is the sum of the products of RMS phase voltage and RMS phase current measured from each line to neutral:

$$S_T = 3\ V_{L-N}\ I_{L-N}$$

or in terms of RMS line voltage and RMS line currents:

$$S_L = \sqrt{3}\ V_L I_L$$

b) The active, real or effective power (P) is that component of apparent power which is dissipated either in a load or as loss.

c) Reactive power (Q_T) is that component of apparent power which contributes to the total volt amperes of a system but not to active power.

d) The system power factor is the ratio of the active power to the apparent power, it is also the cosine of the angle (θ) between the apparent power and the active power. These criteria are illustrated in Figure A-1 which is a phasor diagram of a power system.

In a balanced three-phase system, where currents and voltages are sinusoidal and of the same frequency, the power characteristics can be completely determined using the two-wattmeter method. Because the wattmeters are sensitive to the product of the current, the voltage and the phase angle between them, the individual wattmeter outputs can be used to calculate active power, reactive power, power factor and apparent power using the following formulas:

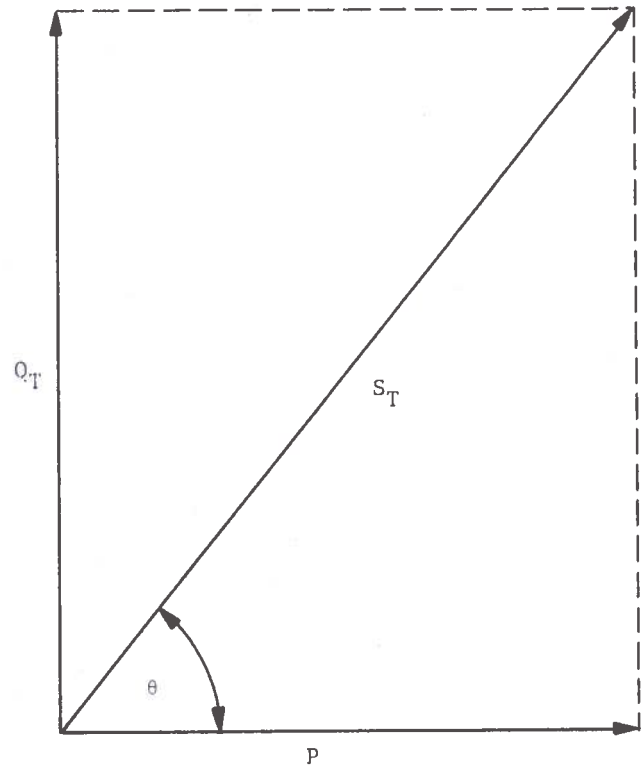

Figure A-1. Phasor Diagram of Total Power Components

$$P = W_1 + W_2$$

$$Q = \sqrt{3}\ (W_1 - W_2)$$

$$\tan \theta = \frac{P}{Q}$$

$$pf = \cos \theta$$

$$S = \frac{P}{\cos \theta}$$

where W_1, W_2 = wattmeter readings

P = active power

Q = reactive power

S = apparent power

pf = system power factor

θ = system power factor angle, which is the angle between applied voltage and current.

Rectifier systems, in which the line currents are abruptly switched or chopped, may contain harmonic distortion components of current, voltage or both. For these systems, significant measurement errors result if only wattmeters are used to measure the power characteristics. To characterize these systems, the following measurements are required: active power, apparent power, displacement reactive power, distortion reactive power and system power factor. Some of these parameters are available through direct measurement but the remainder can only be determined through indirect measurements. The following formulas can be used to obtain the complete power characteristics of a three-phase system.

Active Power: $P = W_1 + W_2$

Total Apparent Power: $S_T = \sqrt{3}\ V_L\ I_L$

System Power Factor: $\frac{P}{S_T} = \cos\theta$

Total Reactive Power: $Q_T = S_T \sin\theta$

Phase Displacement Reactive Power: $Q_P = \sqrt{3}\ (W_1 - W_2)$

Distortion Reactive Power: $Q_d = \sqrt{Q_T^2 - Q_P^2}$

Note also that the Total Reactive Power: $Q_T = \sqrt{Q_P^2 + Q_d^2}$

The active power can be measured with two wattmeters, providing their bandwidth includes all of the harmonics that are present. The wattmeters give the solution to the integral

$$W = \frac{1}{T} \int_0^T v(t)i(t)dt$$

and give a true reading of power regardless of the degree of unbalance and distortion. The RMS voltage and RMS current measurements must be made with true RMS reading instruments.

A discussion of power system characteristics for non-sinusoidal conditions is given in the following section.

A-2 MEASUREMENT OF NON-SINUSOIDAL WAVEFORMS

There is a power factor associated with a rectifier or chopper system which is the result of either or both of two phenomena.

a) The delay of thyristor turn-on in PDR systems results in a phase displacement of the current and voltage waveforms and hence a displacement component of power factor.

b) The chopping action of rectifier systems generates harmonic currents which distort the waveforms and produce a distortion component of power factor.

The current and voltage can be expressed in terms of the fundamental, its harmonics and displacement angles,

$$v(t) = \sum_{m=1}^{\infty} E_{pm} \sin(m\omega t)$$

$$i(t) = \sum_{n=1}^{\infty} I_{pn} \sin(n\omega t+\psi)$$

and the integral for average power can be rewritten

$$W = \frac{1}{T} \int_{o}^{T} \sum_{\substack{n=1 \\ m=1}}^{\infty} E_{pm} \sin(m\omega t) \cdot I_{pn} \sin(n\omega t+\psi) \, d\omega t$$

This integral has a non-zero solution only for the cases where m=n.

Figure A-2 is a phasor diagram of the power components which can be constructed from data taken with two wattmeters. It does not completely describe the power characteristics of the system with harmonics. All of the components in Figure A-2 result from currents and voltages of the same frequencies. The apparent power, S_p, associated with these quantities can be resolved into its

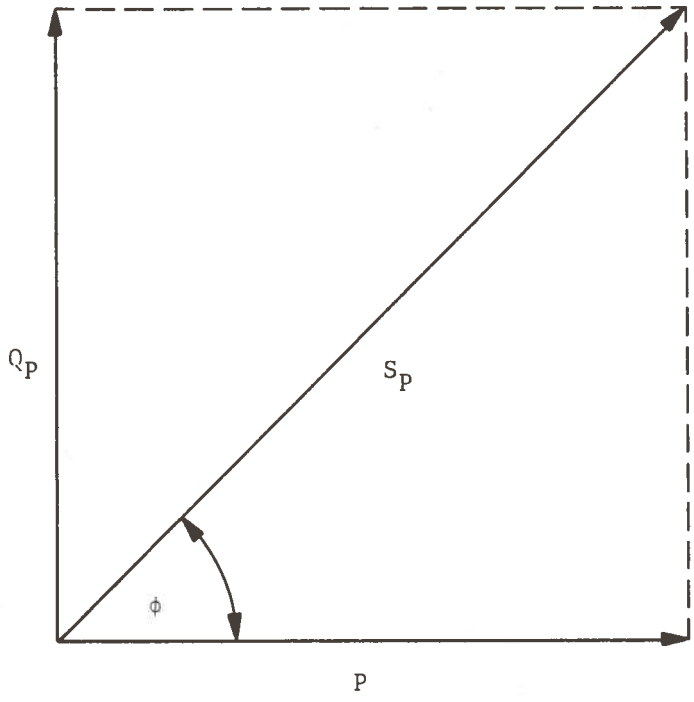

Figure A-2. Phasor Diagram of Power Components from Two-Wattmeter Measurements

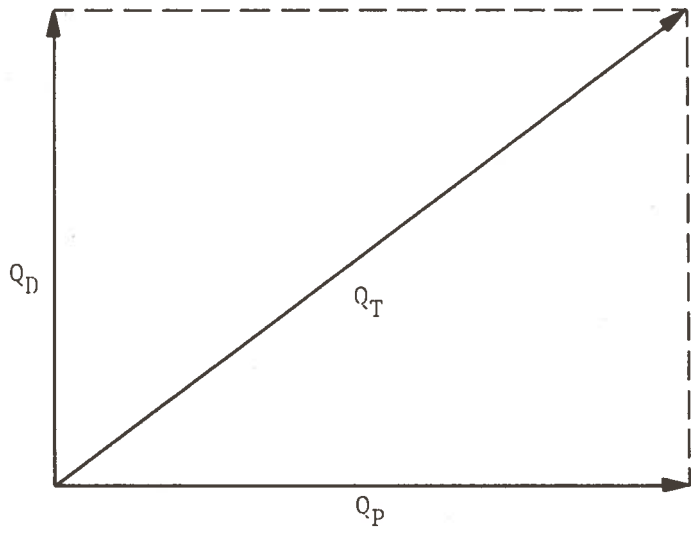

Figure A-3. Phasor Diagram of Reactive Power Components

components: the active power, P, and a reactive power component, Q_p, which results from the phase displacement of the currents and voltages. The angle, ϕ, is the displacement or phase angle between the active power and S_p.

For the case where the input voltage waveform contains only the fundamental frequency and no harmonics, then the angle ϕ is the angle between the active power of the fundamental and the apparent power of the fundamental. It is also the displacement angle between the fundamental voltage and the fundamental current. The cosine of this angle is the displacement power factor which is measured by commerical watt-hour and var-hour meters.

The displacement angle varies with the delay interval in phase delay rectifiers. Addition of inductive filtering to a rectifier output increases the current phase lag and results in a lower displacement power factor.

The presence of harmonics in the line current must also be considered in characterizing a power system. Since the harmonics do not contribute to active power, and since they do contribute to apparent power, the harmonic or distortion component of power must be considered as a component of reactive power. Note that the displacement power factor is the same as the system power factor only for sinusoidal conditions.

The RMS quantities which are used to calculate total apparent power contain both fundamental and harmonic components. These components combine vectorially to produce the RMS line currents and voltages; e.g.,

$$I_L = \sqrt{\sum_{n=1}^{\infty} I_n^2}$$

where I_L = RMS line current
n = order of harmonic
I_n = RMS value of nth harmonic

Since the harmonic distortion components contribute to the total RMS value vectorially, the distortion components also

contribute to total reactive power vectorially. This is illustrated in Figure A-3 which is a phasor diagram of the displacement and distortion components of reactive power. The resultant reactive power (Q_t) is equal to the total system reactive power shown in the total power phasor diagram, Figure A-1.

A pictorial presentation of the power components and how they combine is presented in Figure A-4. The total system apparent power consists of three mutually orthogonal components: active power, phase displacement reactive power and distortion reactive power. All three components must be known to completely characterize the system.

A-3 MEASUREMENT OF POWER SYSTEM COMPONENTS

In a three-phase system, two wattmeters can be used to measure the active power for all conditions of load balance and waveform distortion. The total system apparent power can be determined from the true RMS current and true RMS voltage measurements.

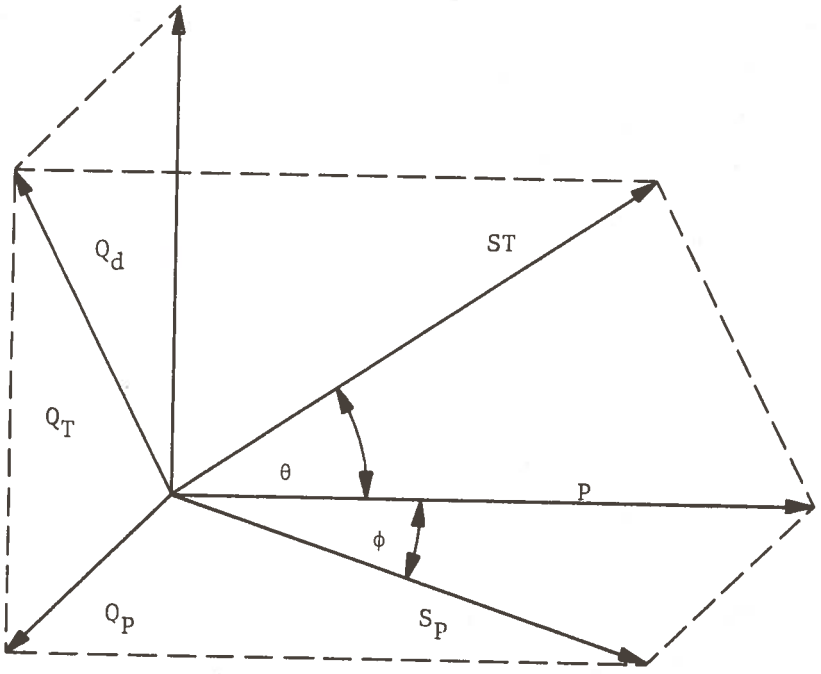

Figure A-4. Phasor Diagrams of Total System Power Components

The total power and the total apparent power measurements can be used to determine the system power factor and total reactive power

$$pf = \frac{W_1 + W_2}{\sqrt{3}\ V_L\ I_L} = \cos\ \theta$$

$$Q_T = \sqrt{3}\ V_L\ I_L \sin\ \theta$$

The two-wattmeter readings can also be used to determine displacement reactive power

$$Q_p = \sqrt{3}\ (W_1 - W_2)$$

The distortion reactive power can then be calculated from

$$Q_d = \sqrt{Q_T^2 - Q_p^2}$$

The instrumentation required to accomplish these measurements will depend on the volume of data to be analyzed. In either a laboratory or field environment, the instrumentation should have a response bandwidth wide enough to encompass the highest harmonics of both voltage and current without introducing additional distortion. This criteria should be closely investigated when dealing with variable-frequency power systems. The following instruments are necessary:

1. one pair of wide-band wattmeters
2. true RMS indicating voltmeters
3. true RMS indicating ammeters

With these instruments, the system power characteristics can be determined as summarized above.

For a more complete determination of system power characteristics the following additional instruments are recommended.

1. wave analyzer, to determine the order and magnitude of individual harmonics

2. distortion analyzer, to determine the total harmonic distortion which then can be used to calculate the distortion reactive power

3. real-time wave analyzer with parallel outputs for monitoring transient harmonic phenomena.

Systems which are at field locations or which require a large volume of data for system analysis are better instrumented with transducers rather than meters. The transducers will present an output signal proportional to the parameter being monitored. This signal can then be displayed on an oscilloscope for real-time analysis, on a strip chart for near real-time analysis or it can be recorded on an instrumentation tape recorder for future digitization and computer analysis or to produce additional strip chart records.

In addition to transducers which meter individual system parameters, an arithmetic function module should be included. This module can be instrumented to perform the arithmetic operations for calculation of system power characteristics. Inputs to the module as well as parameters to be monitored may vary from system to system depending on system analysis requirements, however the following transducers and instruments should provide the necessary data for complete power system characterization.

1. true RMS voltage transducers

2. true RMS current transducers

3. wattmeter transducers

4. harmonic distortion analyzer, with analog outputs

5. wave analyzer, with analog outputs

6. real-time wave analyzer, with analog outputs

7. arithmetic function module.

The outputs of the first six instrument types can be used to monitor the individual parameters and they can also be fed into the arithmetic function module where operational circuits will

perform the necessary arithmetic computations to provide outputs proportional to:

1. total apparent power
2. system power factor
3. total reactive power
4. harmonic-to-fundamental ratios for each harmonic.

Additional outputs from the AFM can be implemented as the requirements for the measurement arise.